

Publisher source acknowledgment:

<https://doi.org/10.1016/j.ejmech.2022.114358> (final version)

Structure-based design of novel donepezil-like hybrids for a multi-target approach to the therapy of Alzheimer's disease

Leonardo Brunetti^{a,b,#}, Rosalba Leuci^{a,#}, Antonio Carrieri^a, Marco Catto^a, Sara Occhineri^a, Giuseppe Vinci^a, Lucia Gambacorta^c, Hanna Baltrukevich^{a,d}, Sílvia Chaves^b, Antonio Laghezza^a, Cosimo Damiano Altomare^a, Paolo Tortorella^a, M. Amélia Santos^b, Fulvio Loiodice^a and Luca Piemontese^{a,*}.

^a *Department of Pharmacy—Pharmaceutical Sciences, University of Bari Aldo Moro, via E. Orabona 4, 70125 Bari, Italy*

^b *Centro de Química Estrutural, Institute of Molecular Sciences, Departamento de Engenharia Química, Instituto Superior Técnico, Universidade de Lisboa, Av. Rovisco Pais 1, 1049-001 Lisboa, Portugal*

^c *Institute of Science of Food Production—ISPA, Research National Council—CNR, Via Amendola, 122/O, 70126 Bari, Italy*

^d *Faculty of Pharmacy, Chair of Technology and Biotechnology of Medical Remedies, Jagiellonian University Medical College in Krakow, Medyczna 9, 30-688 Kraków, Poland*

The two authors (Leonardo Brunetti and Rosalba Leuci) contributed equally to this work.

* Corresponding author: luca.piemontese@uniba.it

Abstract

Alzheimer's disease (AD) is a widespread multifactorial aging-related pathology, which includes cholinergic deficit among its main causes. Following a multi-target design strategy, the structure of the approved drug donepezil was taken as the starting point for generating some new potential multi-functional compounds. Therefore, a series of twenty molecular hybrids were synthesized and assayed against three different enzymes, namely the well-established targets acetylcholinesterase (AChE) and butyrylcholinesterase (BChE), and the innovative one fatty acid amide hydrolase (FAAH). *In silico* studies confirmed the interaction of benzylpiperidine and the benzylpiperazine isostere with the catalytic anionic site (CAS) of AChE, while the aryloxycarbonyl portion appeared to be important for the interaction with the peripheral site (PAS). A QSAR study was carried out on AChE inhibition data, which revealed that the inhibition potency seems to depend upon the length of the spacer and the number of polar atoms. The docking poses of selected compounds within BChE and FAAH were also calculated. Furthermore, pharmacokinetics and drug-likeness properties were assessed by chemoinformatic tools. Several piperidine derivatives (in particular compound **10**) showed interesting profiles as multi-target directed agents, while the lead piperazine derivative **12** (**SON38**) was found to be a more potent and selective AChE inhibitor ($IC_{50} = 0.8$ nM) than donepezil, besides being able to bind bivalent copper cations ($pCu = 7.9$ at physiological pH). Finally, the selected lead compounds (**10** and **12**) did not show significant cytotoxicity on SH-SY5Y and HepG2 cells at the highest tested concentration (100 μ M) in a MTT assay.

Keywords: Alzheimer's disease; neurodegeneration; multifunctional drugs; donepezil; FAAH; acetylcholinesterase; butyrylcholinesterase; docking; QSAR; chelating agents.

Introduction

Over the last few decades, the standards of living have been increasing worldwide. As a result, life expectancies have risen as well, leading to a demographic shift towards older age groups, especially in developed countries. Consequently, illnesses that predominantly affect the elderly have also been steadily increasing in prevalence, among which Alzheimer's disease (AD) is poised to become one of the most relevant. AD starts ca 20 years before the first signs occur and it is a form of dementia whose main clinical symptoms are related to the loss of important cognitive functions such as memory and language, and the costs, both emotional and economic, related to the care of AD patients are significant [1].

Historically, the molecular hallmarks of AD have been identified as a result of a reduction in cholinergic neurotransmission linked to lower acetylcholine (ACh) levels. Among other common AD pathophysiological factors are the accumulation of β -amyloid ($A\beta$) aggregates (senile plaques), and the formation of neurofibrillary tangles of hyperphosphorylated tau protein [2]. It is important to note that neurodegenerative processes and $A\beta$ plaques themselves induce increased levels of inflammatory mediators, leading to oxidative stress and driving further the progression of the disease [3].

It has also been shown that metal dyshomeostasis, meaning an excess of essential biometal ions (mainly Cu, Fe and Zn), in certain brain compartments can have neurotoxic effects. This phenomenon has been strongly linked to the etiology of neurodegenerative diseases, including AD, for a long time, and it is thought to play an important role in amyloid plaque formation [4]. Both the redox-active metal ions (Cu and Fe) can participate in oxidative reactions, generating reactive oxygen species (ROS), which can in turn trigger a cascade of pathological events and induce the formation of toxic misfolded protein aggregates, in particular with formation of copper-amyloid complexes [5,6]. The redox inert zinc plays a dynamic role in the physiology and pathophysiology of brain functions, being mostly bound in metal-protein complexes to achieve enzymatic activity [7]. The connection between AD and metal dysregulation was proven by *post-mortem* analyses of amyloid plaques that evidenced accumulation of copper, iron and zinc whose levels were

respectively 5.7, 2.8 and 3.1 times higher than found in healthy brains [8]. Therefore, targeting metal dyshomeostasis has been elected as a potential strategy for AD therapy [9,10], and numerous metal chelating agents, in particular copper chelators, have been developed to remove or inactivate the metal neurotoxic participation either in redox-active reactions or in the aggregation of misfolded proteins [11].

More recent studies have also shown how insulin-resistance and impaired glucose metabolism (themselves strongly linked to neuroinflammation) correlate with lower A β degradation in microglia and neurons, adding a new layer to the etiology of AD [12,13]. In this context, the endocannabinoid system (ECS) has become an increasingly interesting therapeutic target, seeing how cannabinoid receptors (CBRs) CB1 and CB2 are expressed in the central nervous system (CNS) and their activation inhibits the production of proinflammatory cytokines [14–16]. Moreover, the main endocannabinoid Anandamide (arachidonoyl-ethanolamine, AEA) has been shown to be less concentrated in the brain of AD patients, with its concentration being negatively correlated with the quantity of A β [17]. Other than being the main endogenous ligand of the CBRs, AEA is also an agonist of the Peroxisome proliferator-activated receptor gamma (PPAR γ), whose activation has insulin-sensitizing effects, and related compounds such as palmitoyl-ethanolamine (PEA), sharing common biosynthetic and catabolic pathways with AEA, are similarly active as endogenous agonists of PPAR α . While PPARs are generally understood as key regulators of lipid and carbohydrate metabolism, they (PPAR α in particular) are also involved in anti-inflammatory processes, and thus could be an important innovative target for the treatment of AD [18–23]. The degradation of AEA and its congeners is mediated by enzyme Fatty Acid Amide Hydrolase (FAAH), whose expression is significantly elevated in astrocytes and microglia associated with neuritic plaques, leading to higher local concentrations of arachidonic acid which, being the substrate for the synthesis of prostaglandins, further drives neuroinflammation [17,24]. Administration of FAAH inhibitors is associated with reduced levels of ROS, prostaglandins and pro-inflammatory cytokines. These effects in particular are mediated by activation of vanilloid

receptor 1 (TRPV1), which results in suppression of enzymes cyclooxygenase-2 and inducible nitric oxide synthase, and are compounded by the further anti-inflammatory effects of CBR and PPAR activation [21,25]. The neuroprotective effects of FAAH inhibition have been demonstrated in the animal model, and this particular innovative therapeutic strategy has shown a safe clinical profile in humans, leading to significant research interest towards the development of FAAH inhibitors that could be deployed in the treatment of AD [21,26–28].

Although clear progress has been made, it must be remarked that the pathogenesis of AD is still largely uncertain, and while a few drugs have been approved for its treatment, their action is largely symptomatic, merely delaying the disease's inevitable and painful consequences [29]. However, it is critical to note that these drugs, mostly inhibitors of acetylcholinesterase (AChE), only focus on a single target. Indeed, due to the limited effectiveness of these drugs, it has become increasingly clear that the multi-factorial nature of AD implies that its therapy should tackle multiple disease targets. For this reason, the development of multi-target therapeutic agents has garnered increasing interest, becoming the new paradigm for research in this field in the last decade [11,30–32].

Following such a multi-target approach, we set our sights on the regulation of both cholinergic transmission and endocannabinoid tone, with our main strategy being enzyme inhibition, namely of AChE, butyrylcholinesterase (BChE) and FAAH. While cholinesterases, and AChE in particular, are well-established targets for AD therapy [30,33], FAAH inhibition is a much more recent development, aimed at increasing the concentration of Anandamide and its congeners such as PEA in the CNS, with reduced neuroinflammation and improved neurotrophic function caused by indirect activation of CBRs and PPARs as possible mechanisms of action [21,34,35].

Based on a recent screening conducted on a set of aryloxyacetic acids previously synthesized by our research group, we found that such a scaffold could bind quite easily to FAAH, likely to its Membrane Access Channel (MAC) [36]. Due to several recently recognized structural similarities between cholinesterases and FAAH [34], we have developed molecular hybrids (**1-20**, Figure 1) containing both an aryloxyacetic moiety and a donepezil-like benzylpiperidine or benzylpiperazine

isostere moiety, with structural variations encompassing both the aromatic portion of the former, and the length of the linker between the two moieties themselves. In this case, we decided to use a one or two methylene chain linker, as optimized in our recent published studies [37–39]. The biological activities of these compounds were evaluated as AChE, BChE and FAAH inhibition. Considering the wide range of AChE inhibition data, a QSAR study was carried out, and a subsequent structure-based study was performed by dockings of selected compounds into the catalytic site of this enzyme as well as BChE and FAAH. Moreover, docking studies suggested a possible intramolecular hydrogen bond to achieve a proper bioactive conformation producing a significant activity against AChE, evident in a couple of hybrids (**12** or **SON38** and **13**). This conformation seemed to be also useful for a potential interaction of some of these molecules with selected heavy metals. Therefore, we explored this possibility for the most interesting compound **12** (**SON38**) by evaluating its ability to chelate copper (II), whose dyshomeostasis is involved in neurotoxicity. Finally, drug-likeness predictions were performed in order to address the pharmacokinetic properties on the most interesting compounds.

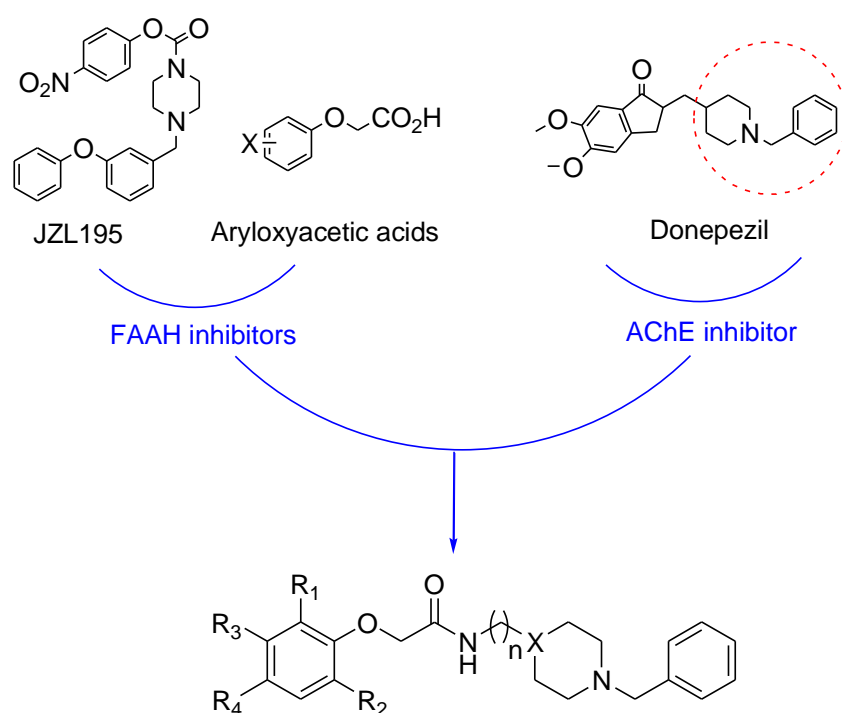


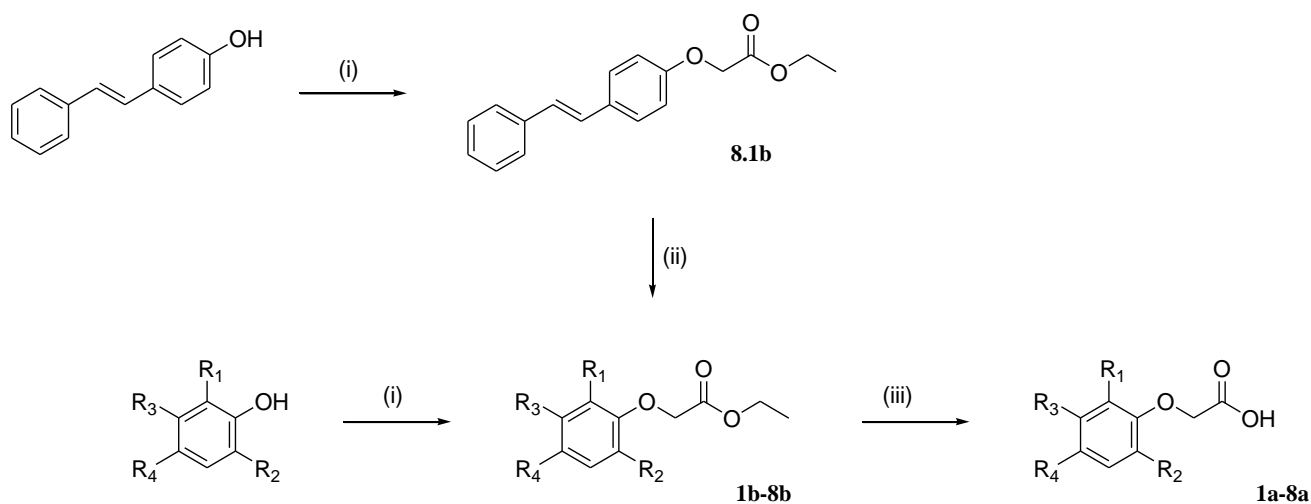
Figure 1. Drug design for the hybrids **1-20**.

Results

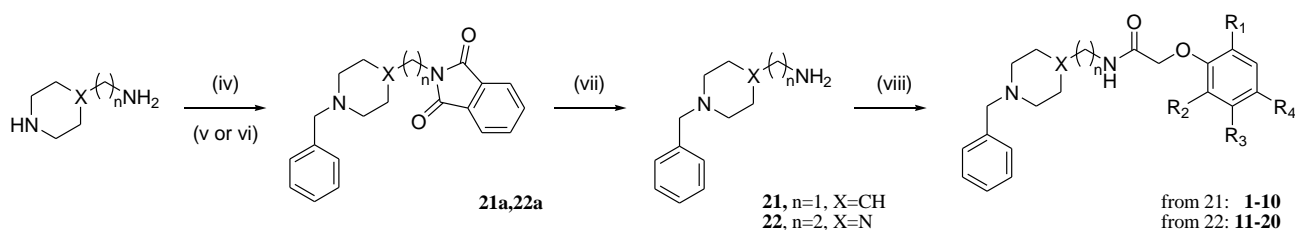
Chemistry

The intermediates **1b-7b** were prepared according to previously reported procedures [36] (**Scheme 1**), starting from the suitable commercial substituted phenols and ethyl bromoacetate, using sodium ethoxide as a base. *Trans*-4-styrylphenol was condensed with ethyl bromoacetate affording compound **8.1b**, whose catalytic hydrogenation led to compound **8b**. Intermediates **1a-8a** were obtained by hydrolysis of **1b-8b** under basic conditions.

Scheme 2 describes the synthesis of title compounds **1-20** (Figure 1). The primary alkylamine group of commercial 4-(aminomethyl)piperidine or 1-(2-aminoethyl)piperazine was protected by a neat reaction with phthalic anhydride at 160 °C [40]. *N*-benzylation of the cyclic amine involved a reaction with benzyl bromide under basic conditions. Free amines **21** and **22** were obtained through deprotection with aqueous solution of methylamine 40% (*w/w*) [41]. Final ligands **1-10** and **11-20** were obtained by condensation between the carboxylic groups of **1a-10a** (**9a** and **10a** were commercially available) and the primary amine group of **21** or **22**, respectively, using 1-hydroxybenzotriazole hydrate (HOBt) and *N,N'*-diisopropylcarbodiimide (DIC) as condensing agents [42].



Scheme 1. i) Na, abs EtOH, ethyl bromoacetate, reflux, 23 h; (ii) H₂, Wilkinson's catalyst, THF/EtOH, RT, 48 h; (iii) 1 N NaOH, THF, RT, 5 h.



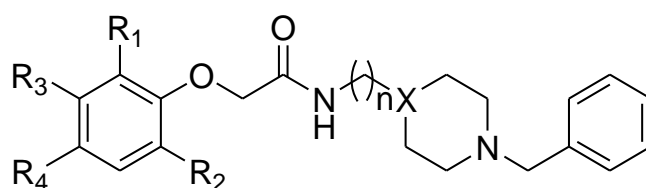
Scheme 2. iv) phthalic anhydride, 160 °C, 4 h; v) benzyl bromide, triethylamine, 96° ethanol, RT, 24 h; vi) benzyl bromide, KOH, 96° ethanol, RT, 24 h; vii) aq solution of MeNH₂ (40% w/w), RT, 72 h; viii) **1a-10a**, DIC, HOBt, CH₂Cl₂, RT, 16 h.

Biological Assays

In this study, the substituents introduced in the phenoxy group of compounds **1-20** were selected based on their different stereoelectronic properties and commercial availability. A preliminary docking evaluation was also performed (data not shown). The ability of these molecules to inhibit

the enzymes AChE, BChE and FAAH is reported in Table 1 as IC₅₀ (μM) or as a percentage of inhibition at a fixed ligand concentration (10 μM). Donepezil and JZL195 were used as reference compounds for ChEs and FAAH, respectively.

Table 1: Biological activities of compounds **1-20** towards AChE, BChE and FAAH



Compound	X	n	R ₁	R ₂	R ₃	R ₄	IC ₅₀ , μM ^a		
							<i>h</i> AChE	<i>h</i> BChE	<i>h</i> FAAH
1	CH	1	H	H	H	Ph	1.70 ± 0.13	5.58 ± 0.29	23.3 ± 2.1
2	CH	1	H	NO ₂	H	Cl	0.122 ± 0.001	4.70 ± 0.14	23.3 ± 4.6
3	CH	1	H	NO ₂	F	H	0.103 ± 0.013	54 ± 2 % ^b	28.1 ± 0.6
4	CH	1	H	H	H	NO ₂	0.509 ± 0.014	24 ± 3 % ^b	28.5 ± 8.0
5	CH	1	H	CF ₃	H	H	0.767 ± 0.032	1.02 ± 0.06	38.2 ± 15.0
6	CH	1	CH ₃	CH ₃	H	Br	0.595 ± 0.039	2.22 ± 0.25	28.6 ± 7.4
7	CH	1	H	H	H	CH ₂ Ph	1.27 ± 0.07	37 ± 2 % ^b	21.9 ± 6.1
8	CH	1	H	H	H	CH ₂ CH ₂ Ph	0.135 ± 0.008	5.08 ± 0.09	23.8 ± 4.0
9	CH	1	H	H	H	OCH ₃	0.880 ± 0.007	55 ± 5 % ^b	40.8 ± 7.3
10	CH	1	H	H	H	Cl	1.68 ± 0.14	5.61 ± 0.23	20.9 ± 0.6
11	N	2	H	H	H	Ph	0.735 ± 0.004	0.969 ± 0.053	63.9 ± 8.9
12	N	2	H	NO ₂	H	Cl	0.0008 ± 0.0002	1.41 ± 0.27	41.6 ± 7.4

13	N	2	H	NO ₂	F	H	0.0028 ± 0.0002	5.01 ± 0.12	49.6 ± 12.7
14	N	2	H	H	H	NO ₂	0.042 ± 0.012	n.a. ^b	43.9 ± 5.5
15	N	2	H	CF ₃	H	H	0.136 ± 0.008	0.503 ± 0.014	55.1 ± 11.1
16	N	2	CH ₃	CH ₃	H	Br	0.090 ± 0.020	4.10 ± 0.14	40.8 ± 6.8
17	N	2	H	H	H	CH ₂ Ph	0.993 ± 0.101	29 ± 4 % ^b	23.6 ± 2.4
18	N	2	H	H	H	CH ₂ CH ₂ Ph	0.900 ± 0.057	45 ± 2 % ^b	16.8 ± 6.2
19	N	2	H	H	H	OCH ₃	0.300 ± 0.009	25 ± 2 % ^b	51.9 ± 18.0
20	N	2	H	H	H	Cl	0.189 ± 0.012	2.15 ± 0.09	>100
Donepezil							0.017 ± 0.002	4.80 ± 1.00	n.d.
JZL195							n.d.	n.d.	0.019 ± 0.003

(^a) Values are mean ± SEM; (^b) % inhibition at 10 μM; n.a = not active, n.d. = not determined

The piperidine series (**1-10**) shows good inhibition of cholinesterases; in particular, IC₅₀ values towards AChE are comprised in a limited range, between low micromolar and high nanomolar values (0.10-1.70 μM). Moreover, the presence of the nitro substituent on the phenoxy ring (compounds **2-4**) supports the anticholinesterase activity, probably due to electronic effects, considering that the presence of an additional electron withdrawing group leads to the lowest IC₅₀ values among this piperidine series (compounds **2** and **3**). The same relative order of inhibitory capacity is kept regarding BChE, although the potency of these compounds as BChE inhibitors is generally lower (IC₅₀ = 4.70 μM for **2**, 54% inhibition at 10 μM for **3** and 24% of inhibition at 10 μM for **4**).

Among this subset of compounds, it is important to note that when bulky substituents are introduced in position 4 of the phenoxy (**1,7** and **8**), the distance between the two phenyl groups

seems to be essential: compound **8**, which has an ethylene linker, is one order of magnitude more potent towards AChE than **1** and **7** and is slightly more effective than **1** towards BChE as well.

In general, all compounds in the **1-10** series show lower inhibition of BChE. The best results regarding the inhibition of BChE are achieved by compounds that are functionalized in position 2, particularly when the substituents are not bulky (**5** and **6** with CF₃ and CH₃ in position 2 and IC₅₀ of 1.02 and 2.22 μM, respectively).

The piperazine series (**11-20**) exhibits marked potencies toward acetylcholinesterase, with IC₅₀ values in a wide nanomolar range covering four orders of magnitude (0.8-993 nM). Again, the nitro group as substituent in compounds **12-14** is responsible for an increase in the activity against AChE, leading to molecules (e.g. **12** and **13**) up to 21 times more active than the reference compound donepezil, one of the few anticholinesterase drugs currently used in AD therapy. The importance of a substituent in *ortho* position with respect to the phenoxy oxygen atom, together with an additional electron withdrawing atom, is confirmed by the data obtained for compound **16**, which keeps a good anti-AChE activity, although it is around two orders of magnitude less potent than **12**.

Compounds that have slightly weaker electron withdrawing properties (e.g. **15** and **20**) still show significant activity, while the only compound in the series bearing a strong electron-donor group (molecule **19**) results about four hundred times less potent than the best analogue of the series (molecule **12**, **SON38**) considering AChE as a single target.

In relation to steric effects, on the other hand, a lower anticholinesterase activity is observed (up to four orders of magnitude compared to **12**) in compounds with bulky substituents in position 4 of the phenoxy (**11**, **17** and **18**).

Compound **11** also shows good inhibitory activity towards BChE (IC₅₀ = 0.969 μM), comparable to the value found for AChE (IC₅₀ = 0.735 μM). Regarding BChE inhibition, all compounds of the

piperazine series (**11-20**) show higher IC_{50} values. Nevertheless, they partially confirm the efficacy of the *ortho*-substitution of the phenoxy ring, with compounds **15** and **12** among the best in the series ($IC_{50} = 0.503$ and $1.41 \mu\text{M}$, respectively), probably due to the presence of a small and electron withdrawing group, whose importance is evident also in the piperidine series (compound **5**, $IC_{50} = 1.02 \mu\text{M}$).

As regards FAAH inhibition, which was measured via a fluorometric enzyme assay, the data found for the piperidine series (**1-10**) is promising and within a relatively short range (IC_{50} 20.9-40.8 μM), probably because the proposed substituents are far from the possible pharmacophore portion. The IC_{50} values obtained for piperazines (**11-20**) are also in the micromolar range (16.8-63.9 μM , except for compound **20**). For this series, the presence of two suitably spaced phenyl groups makes compound **18** the best of the series (16.8 μM), especially when compared with compound **11**, in which the phenyl is directly bound to the phenoxy, which is instead among the worst tested compounds (63.9 μM). The corresponding behaviour, involving bulky substituents in piperidine analogues **1**, **7** and **8**, is not observed.

The length and flexibility of these structures may also be a future key to correctly modulate the activities on the different therapeutic targets, with the ultimate goal of obtaining a molecule with a suitable multi-target profile. In fact, the length of the molecules seems important for AChE inhibition as well: all the shorter piperidines are less active than the longer piperazines comparing the molecules bearing the same substituents on the phenoxy ring, except for phenethyl-substituted compounds **8** and **18**: in this case, the piperidine **8** is considerably more potent as AChE inhibitor than the piperazine **18**.

Additional assays were performed on $A\beta_{1-40}$ aggregation *in vitro* (Table S1) [43]. As expected, none of the compounds was particularly effective, lacking the classic structural requirements (planar condensed heterocycles) common to multi-target action compounds previously synthesized and published in the recent past [37,40,44]. Compounds **10**, **14**, and **18-20**, all bearing substituents in

position 4 of the phenoxy group, show however a modest and similar activity (the percentage of inhibition was around 30% at 100 μM in the experimental conditions) [43].

While not showing a marked activity towards a particular target, piperidines (**1-10**) result as promising multi-functional compounds, and **10** shows the best results in regard to their multi-target potential, with good and comparable inhibitory activities towards all three tested enzymes (between 1.68 and 20.9 μM) and a slight ability to interfere in the formation of amyloid aggregates (30% of inhibition at 100 μM). On the other hand, piperazine derivatives (**11-20**) show a marked selectivity towards AChE, with considerable high Selectivity Index (S.I.) values for compounds **12** (**SON38**, S.I. = 1762) and **13** (S.I. = 1789), which result twenty-one- and six-times more active than donepezil, respectively, presenting as well interesting activities towards BChE (compound **12**, **SON38** is three-times more active than donepezil).

In an attempt to place on a more quantitative basis the observed SARs, a regression analysis through the ordinary least-square (OLS) method was carried out on AChE IC_{50} values, which span more than three log units. Seven quick and *easy-to-use* descriptors of lipophilicity, size/polarizability and polarity were calculated (Table S1) and correlated with the enzyme inhibition data expressed as pIC_{50} s. The molecular descriptors were calculated from the single atomic matrix of connections and not by the atomic coordinates, and therefore are conformation independent. The squared correlation matrix (r^2) between pIC_{50} and molecular descriptors (Table 2) shows that, within the limits of the examined molecular space, the only descriptor which somehow correlates with the inhibition potency ($r^2 = 0.60$) is AloNO , which encodes for polarity and hydrogen bond capacity of the ligands.

Table 2 Squared correlation matrix between the calculated molecular descriptors and AChE pIC_{50} values.

<i>pIC50</i>	<i>LogD</i>	<i>PSA</i>	<i>VdW</i>	<i>Refract</i>	<i>Rot</i>	<i>AloNO</i>	<i>Spacer</i>
--------------	-------------	------------	------------	----------------	------------	--------------	---------------

<i>pIC50</i>	1.000							
<i>LogD</i>	0.052	1.000						
<i>PSA</i>	0.482	0.367	1.000					
<i>VdW</i>	0.008	0.799	0.151	1.000				
<i>Refract</i>	0.056	0.839	0.198	0.915	1.000			
<i>Rot</i>	0.020	0.300	0.001	0.527	0.458	1.000		
<i>AloNO</i>	0.601	0.268	0.654	0.176	0.297	0.002	1.000	
<i>Spacer</i>	0.190	0.069	0.007	0.108	0.031	0.266	0.094	1.000

LogD^(a) distribution coefficient *PSA*^(b) polar surface area *VdW*^(b) van der Waals volume *MR*^(c) molar refractivity *Rot*^(d) rotatable bonds *AloNO*^(e) number of halogen, nitrogen and oxygen atoms *Spacer*^(f) alkyl spacer.

Attempts to obtain multiparametric equations through a stepwise regression analysis did not afford any noteworthy equation. Only combining AloNO count with the binary descriptor of the spacer length resulted in an equation with just a better correlation ($r^2 = 0.64$), suggesting that enzymatic inhibition increases with a higher number of polar atoms and with a longer spacer. Statistics are indeed improved ($r^2 = 0.76$) excluding one mere outlier from the data set, namely the trifluoromethyl derivative **15**.

While this chemical *cliché* may most likely affect AChE inhibitory potency, no similar hypotheses can be postulated for BChE and FAAH activity due to the very narrow data range (less than two log units).

Molecular docking calculation

Insights gained from QSAR were further exploited with a structure-based study via dockings of properly selected compounds into the catalytic sites of the studied enzymes. In the very first step AChE was considered since ligands specificity for this esterase has been indeed largely characterized in terms of three residues cluster, namely Ser203, Glu334, His447 for the catalytic triad (CT), Trp86 and Phe338 for the catalytic anionic site (CAS) and Tyr72, Tyr124 and Trp286 for the peripheral anion site (PAS), and they constitute a main door where binders might adopt

outward-inward orientations. Thus, the hAChE/donepezil X-ray complex was enrolled with the aim of studying binding interactions of our novel compounds.

To explore the complementarity of this novel series of compounds with respect to the active site, as well as the molecular similarity with donepezil, compound **12 (SON38)** was primarily selected being the most active inhibitor; to carefully filter the docking poses the **ESP** rule was applied with the following parameters: **FEB** < -10.00, **ΔE** < 2.00, **EFF** < -0.350, **SIM** > 0.800, **POP** > 20/1000 (see methods). As shown in Figure 2, the most active compound **12 (SON38)** mainly spans the base and the opening of the AChE active center gorge; the cationic nitrogen of the piperazine ring bearing the benzyl group produces significant π - π and cation- π interactions with the PAS Trp286 as well as Phe338 and Tyr337, while the rest of the molecular scaffold is oriented towards the main entrance door of the enzyme. Indeed, this pattern fully resembles the similar interaction motif of donepezil as reported by Silva *et al.* [45].

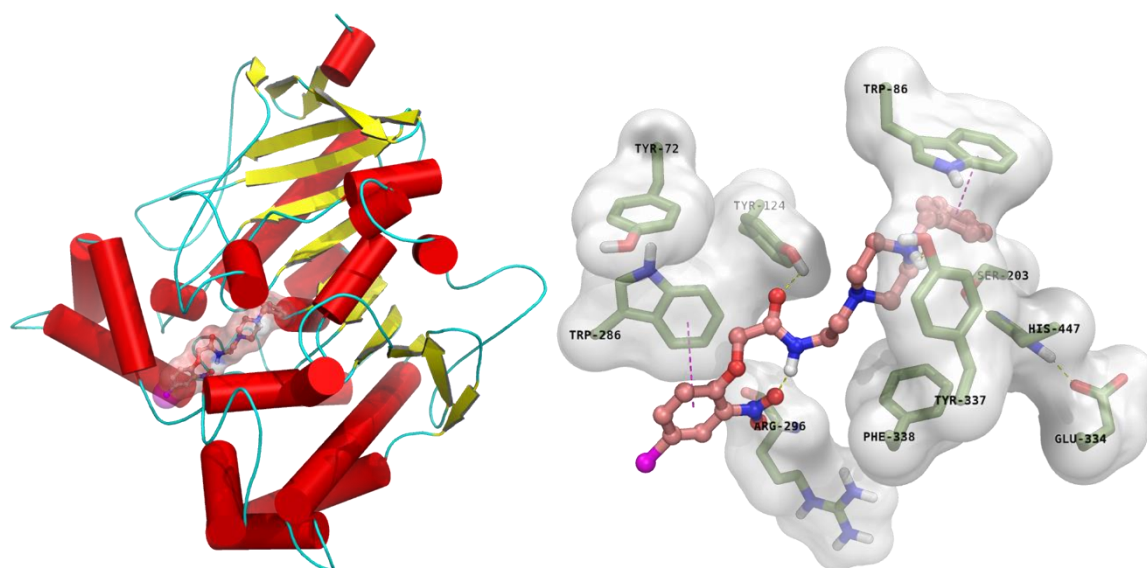


Figure 2. Full (left) and detailed (right) view of the binding mode for compound **12 (SON38)** to the hAChE active site. In the interaction pattern scheme, two hydrogen bonds and π - π stackings are depicted in yellow and magenta respectively.

At the same time, the two carbon atoms long spacer properly lets both the amide and the disubstituted phenyl accommodate into the anionic binding site PAS, with the carbonyl atom and the nitro group recruiting Tyr124 and Arg296 through hydrogen bonds while the aromatic ring generates *face-to-face* π - π stacking with Trp286. It is really intriguing how the intramolecular hydrogen bond allows the whole ligand to assume a proper bioactive conformation, producing a significant activity against AChE. After all, from the docking scoring figures, compound **12** (**SON38**) scored not only highly like donepezil but also showed comparable ligand efficacy (see Table 3).

Table 3. Docking scores for compound **12** compared to donepezil

	FEB ^(a)	ΔE ^(b)	EFF ^(c)	TAN ^(d)	POP ^(e)
12	-11.11	0.29	-0.370	0.818	21/1000
donepezil	-10.30	0.10	-0.368	1.430	508/100

(^a) **FEB** Free Energy of Binding (^b) **ΔE** Energy difference between the selected pose and the relative global minimum (^c) **EFF** Ligand efficacy (^d) **TAN** Tanimoto_Combo similarity coefficient of **12** (**SON38**) with donepezil X-ray pose (^e) **POP** Cluster members population

In light of this evidence, compound **12** (**SON38**) was thereafter taken as inner template to match the binding of some properly selected compounds, namely **2-4**, **8**, **13**, **14**, **18** and **20**, whose chemical decoration deserves interest as a result of the SAR. As it might be perceived from Figure S1, the comparison between the highly active piperazines ($IC_{50} < 0.050 \mu M$) with the less potent, structurally related piperidines ($IC_{50} > 0.100 \mu M$) (i.e. **12** vs **2**, **13** vs **3**, **14** vs **4**) proved that shortening the spacer length would hamper the achievement of the same distinctive interaction pattern of the more efficient IC_{50} values. At the same time, the detrimental effect of the absence of any polar atoms, together with a bulky group at the *para* position, or the importance of the nitro substitution at the *ortho*, are perceivable from the matching of compound **12** (**SON38**) with **8** and **20**. To some extent, differences in ligand efficacy, as scored by dockings, also represent the changes in the observed activities (Table S3).

Slightly different observations were gained from dockings carried out enrolling the BChE X-ray structure (Figure S2): the shape and aminoacidic composition of this different binding site force ligands to adopt a more puckered conformation. In particular, the molecular scaffold is locked in the CAS having the benzyl aromatic terminal pendant π - π stacked against more than one aromatic residue (i.e., Trp82, Trp430, Tyr440), the charged nitrogen making a charged reinforced hydrogen bond with both Asp70 and Tyr332, and the amide embracing a similar bond with Pro285. In addition to this, the substituted phenyl ring points towards Trp231, and it is worth noting that electron withdrawing effect significantly enhances the binding since compound **15** bearing the trifluoromethyl group results one order of magnitude more active than compound **16**.

A similar study was also carried out docking the most active compound **18** to FAAH, and the obtained binding mode is depicted in Figure 3.

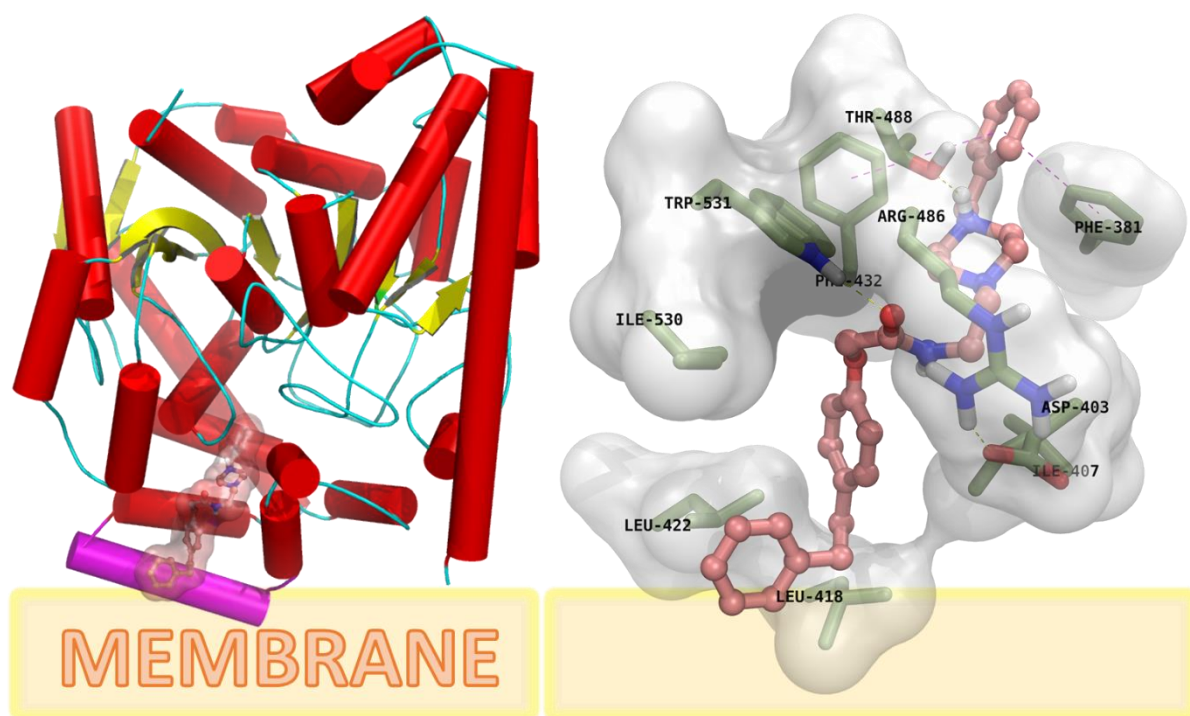


Figure 3 Full (left) and detailed (right) view of the binding mode for compound **18** to the FAAH active site. Hydrogen bonds are depicted in yellow while π - π stackings are in magenta, as well as the parallel helix (see text). The resulting FEB and EFF are -9.04 and -0.266 respectively.

In this instance, the molecular scaffold of the inhibitor is largely placed in a multi-pocket binding site [46,47], although it is not too close to the most critical region of the enzyme (i.e., catalytic triad Ser241, Ser217, Lys142), and this fact might then also explain the very similar, and at the same time moderate, measured inhibition for **18** and the rest of our compounds. Nonetheless, some interesting clues can be perceived and they can rationalize the observed activity: the ligand is indeed sterically adequate to enter and fit the deep FAAH active gorge through the so-called membrane accessing region located just on the top of the extracellular side of the cell membrane, made up of residues (namely Asp403, Ile407, Arg486, Ile530) providing access to compounds characterized by polar head groups. In this binding, the benzyl moiety is directed towards the Phe381 sidechain, and at the same time it makes aromatic contacts with Phe432, which serves, in combination with Trp531, as a dynamic paddling residue, gating the entrance to the catalytic pocket [48]. Likewise, the indole of the same tryptophane, as well as the hydroxyl of Thr488, reinforces the binding due to hydrogen bonds engaging the amide function and the charged nitrogen of piperazine ring, while the phenoxy and its phenethyl pendent return favorable Van der Waals contacts with the Leu418 and Leu 422 part of the parallel helix facing the extracellular side of phospholipidic bilayer.

ADME Properties

Drug-likeness predictions were further gained from the Brain (or IntestinaL Estimate) permeation method [49] which suggests that all studied compounds are well absorbed in the gastrointestinal tract, since their lipophilicity and polarity, measured by WLOGP and TPSA respectively, spot them in the white ellipse of the BOILED-Egg plot (see Figure 4). This graph confirms that the majority of the compounds, including the multitarget promising agent **10**, might be also able to pass the blood brain barrier, but not compounds **12** (SON38) and **13**, which still maintain a good predicted oral adsorption and are not predicted as substrates for P-glycoprotein.

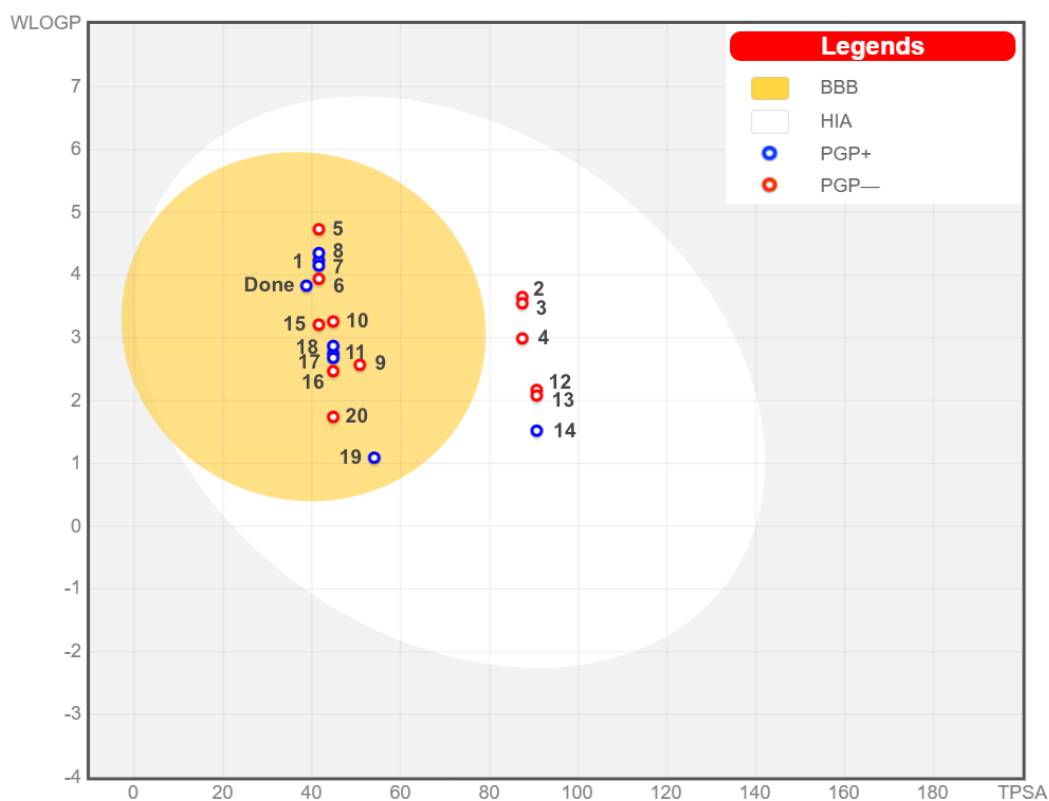


Figure 4. Pharmacokinetic profile of compounds **1-20** according to BoiledEgg. **BBB** = blood-brain barrier permeation; **HIA** = human intestinal absorption; **PGP+** = potential substrate of P-glycoprotein, **PGP-** = non potential substrate of P-glycoprotein.

More pharmacokinetic properties were predicted using QikProp v.2.5, evaluating in particular the compliance of this set of compounds with “Lipinski’s rule of five”, as well as their oral absorption percentage, their CACO-2 cell permeability, their octanol-water partition coefficient (clogP) and their capacity to permeate the BBB. The results are reported in **Table S4**.

This set of aryloxyacetic-donepezil hybrids does not show violations of “Lipinski’s rule of five”, with only two exceptions (compounds **7** and **8** show only one violation). This means that the oral bioavailability of these compounds is potentially high, a fact that is corroborated by the high percentages of predicted oral absorption for all the compounds. The calculated octanol-water partition coefficient (clogP) and the BBB permeability coefficient (log BB) are both well within the acceptable ranges for drug-like compounds (-2 – 6.5 and -3 – 1.2, respectively). The shorter N-

benzyl-piperidine subclass causes higher CACO-2 cell permeability than the longer and more polar N-benzyl-piperazines, suggesting a better profile of intestinal absorption for the former. With a few exceptions (compounds **2-4** and **14**), most of these compounds show high CNS activity, including the most interesting compounds **10**, **12** (SON38) and **13**. Furthermore, desirable physicochemical properties specifically for CNS drugs, such as MW < 450, logP < 5, number of hydrogen bond donors HBD < 3, number of hydrogen bond acceptors HBA < 7 and polar surface area PSA < 60-70 [50] are also fulfilled by several compounds of the piperidine series (**1** and **5-10**), while for all the compounds of the piperazine series (**11-20**) the HBA parameter (7.25-8.25) is slightly above 7 and for **12-14** PSA also shows values above the limit (see Table S4).

Cytotoxicity assays

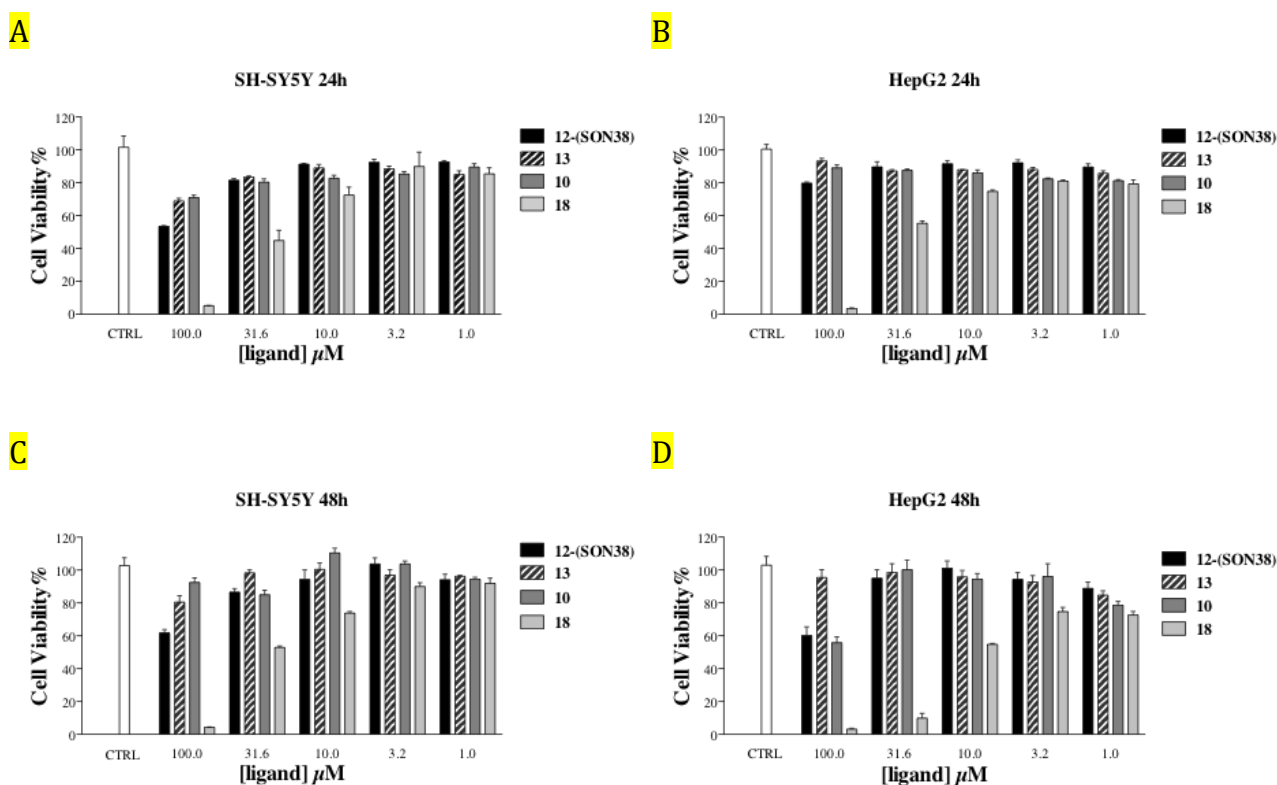


Figure 5. Cell vitality measured by MTT assay. A: SH-SY5Y cells, 24h incubation time; B: HepG2 cells, 24h incubation time; C: SH-SY5Y, 48h incubation time; D: HepG2 cells, 48h incubation time.

The evaluation of the cytotoxicity of a representative selection of this series of donepezil-aryloxyacetic hybrids was conducted via MTT assay using SH-SY5Y neuroblastoma cells and HepG2 hepatocarcinoma cells that were incubated with the tested compounds for either 24 or 48 hours. Specifically, this panel of compounds included **12** and **13** (the most active in the series towards AChE), **10** (with the most favourable multi-target profile) and **18** (most active towards FAAH as a single target). With the exception of compound **18**, the selected molecules did not show relevant cytotoxic effects even at the highest concentration (100 μ M). The moderate cytotoxic effects caused by compound **18** (IC_{50} values shown in Table 4) could be attributed to its higher lipophilicity as predicted via Qikprop (see table S4).

Table 4. IC_{50} values obtained for compounds **10**, **12**, **13** and **18** in the MTT cytotoxicity assays.

ID	SH-SY5Y (IC_{50} μ M)		HepG2 (IC_{50} μ M)	
	24h	48h	24h	48h
10	>100	>100	>100	>100
12	>100	>100	>100	>100
13	>100	>100	>100	>100
18	27.8 \pm 2.7	34.8 \pm 1.9	41.6 \pm 2.9	15.8 \pm 0.6

Copper chelation studies

Besides the inhibitory activity of the herein developed donepezil-based hybrids towards enzymes of interest, their ability to chelate copper, a metal ion with an important role in plaque formation, was also tested in order to preview their potential capacity to interfere with metal dyshomeostasis-related neurotoxicity in AD brains. Therefore, one of the most promising compounds, **12** (SON38), was selected as a model for the piperazine series (compounds **11-20**) and its acid-base properties as well as copper chelating capacity were studied through pH-potentiometric titrations. Due to

solubility limitations, a mixed (30% w/w) DMSO/water medium was chosen for these potentiometric studies. Compound **12** (SON38) was isolated in its neutral form (L, $a = 0$ in **Figure 6**) although it has two dissociable protons (H_2L^{2+}).

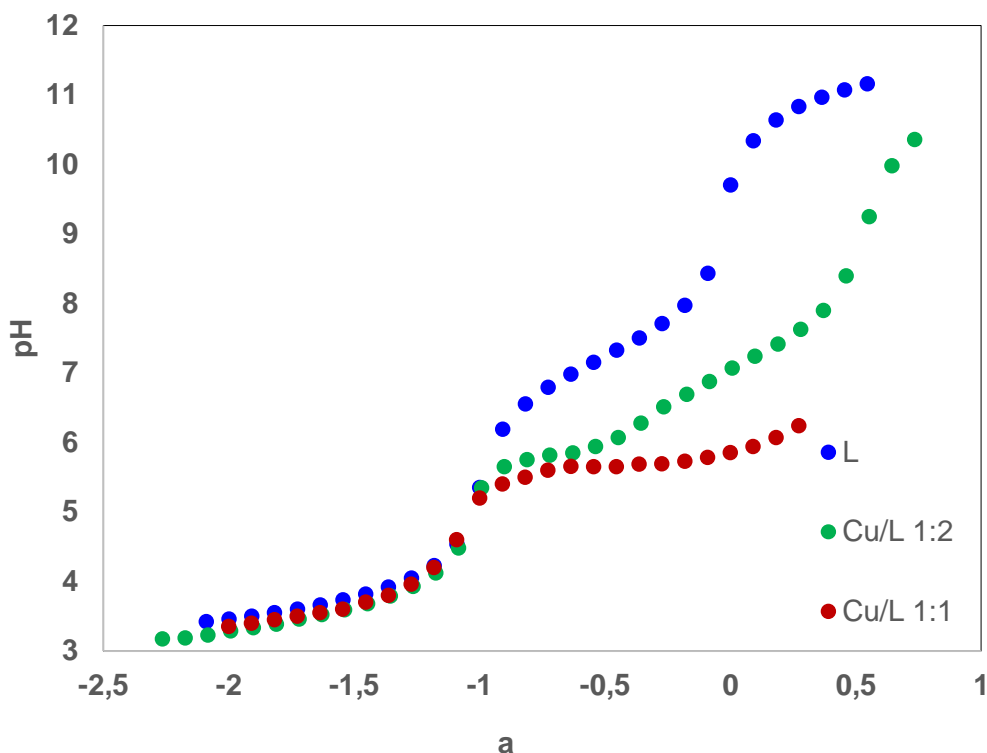
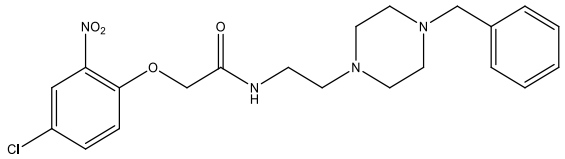


Figure 6. Potentiometric titration curves of **12** (SON38) in 30% DMSO/water medium in the absence or in the presence of Cu^{2+} ($C_L = 5-6.7 \times 10^{-4}$ M, a represents moles of added base per mole of ligand).

The values obtained for the stepwise protonation constants and global formation constants of Cu^{2+} complexes with **12** (SON38) are reported in Table 5 and were obtained by fitting analysis of the experimental pH-potentiometric data with an equilibrium model using Hyperquad 2008 program [51].

Table 5. Stepwise protonation constants ^a of **12** (SON38) as well as global formation constants ^b of its Cu^{2+} complexes and corresponding pCu ^c value. ($T = 25.0 \pm 0.1$ °C, $I = 0.1$ M KCl, 30% w/w DMSO/water).

Compound	$\text{Cu}_m\text{H}_h\text{L}_l$ (mhl)	$\log K_i$	$\log \beta (\text{Cu}_m\text{H}_h\text{L}_l)^a$
 <p>12 (SON38)</p>	(011) (021) (101) (1-11) pCu	7.23(1) 2.89(3) 7.9	 4.94(6) -1.81(7)

^a $K_i = [\text{H}_i\text{L}]/[\text{H}_{i-1}][\text{L}]$; ^b $\beta_{M_mH_hL_l} = [\text{M}_m\text{H}_h\text{L}_l]/[\text{M}]^m[\text{H}]^h[\text{L}]^l$; ^c $\text{pCu} = -\log[\text{Cu}^{2+}]$ at pH 7.4 ($C_L/C_M = 10$, $C_M = 10^{-6}$ M)

The protonation constants depicted in Table 5 correspond to the two ammonium protons of the piperazine unity, being lower than those corresponding to piperazine ($\log K_1 = 9.71$, $\log K_2 = 5.59$ [52]) but analogous to those of piperazine-1,4-bis(*N*-methyl)-acetohydroxamic acid (PIPDMAHA, 6.67, 2.44 [53]) or 1,4-diazacycloheptane-*N,N'*-bis(*N*-methyl)-acetohydroxamic acid (DACHDMAHA, 6.88, 2.93 [54]). The low values obtained for the protonation constants of both PIPDMAHA and DACHDMAHA are explained based on the existence of intramolecular hydrogen bonds between the nitrogen piperazine atoms and the nearby hydroxamate hydroxylic protons forming six-membered rings [53,54]. Therefore, the ammonium protons of these ligands are more acidic than those of piperazine. Concerning compound **12 (SON38)**, the low values presented in Table 5 for the protonation constants can be explained by the existence of two phenomena: coulombic repulsive effects on the *N,N*-diprotonated compound and possible establishment of an intramolecular hydrogen bond between the amide proton and a piperazine nitrogen atom thus forming a five-membered ring.

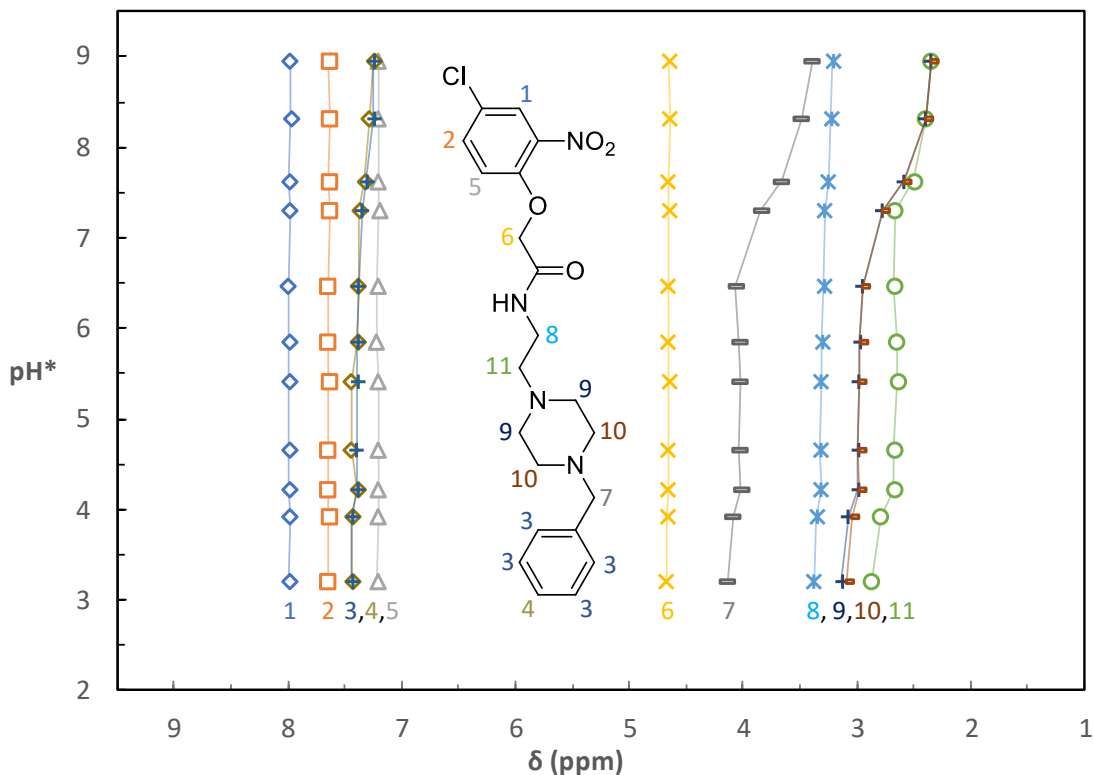


Figure 7. ¹H NMR titration curves of **12** (SON38) in 75% d₆-DMSO/D₂O medium (C_L = 4.5 mM).

The ¹H NMR curves for **12** (SON38), contained in **Figure 7**, show that the triplet corresponding to protons 11, the singlet corresponding to the CH₂ benzylic group (7) and the broad multiplets of protons 9 and 10 show a first downfield shift of the peaks with decreasing pH (pH* 6.5-7.6) and a second one for pH* below 3.9. These downfield shifts are also observed to a much lesser degree for the peaks corresponding to protons 3 and 4. This behavior seems, in fact, in agreement with the protonation of both nitrogen atoms of the piperazine unity. The species distribution curves of compound **12** (SON38, see **Figure 8a**) evidence the major prevalence of the neutral form of the ligand between pH ca 3 and 7, which may be important in terms of biological applications.

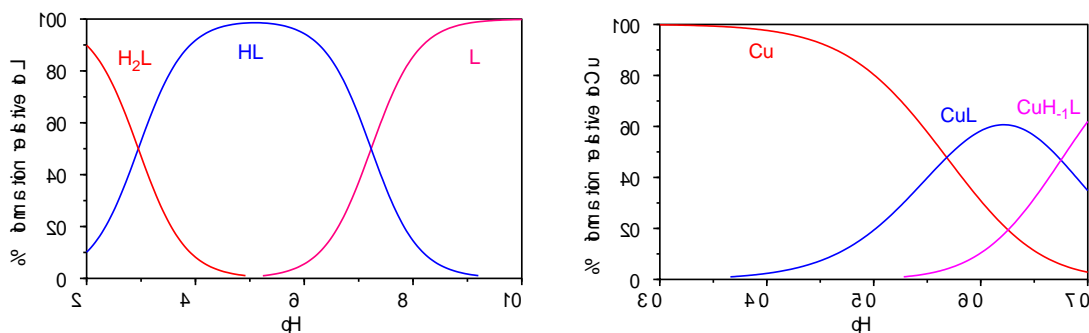


Figure 8. Species distribution curves for a) compound **12** (SON38) and b) $\text{Cu}^{2+}/\mathbf{12}$ (SON38) 1:1 ($C_L = 4.4 \times 10^{-4}$ M).

The copper chelating ability of compound **12** (SON38) was also evaluated by pH-potentiometric titration of the respective 1:1 and 1:2 $\text{Cu}^{2+}/\mathbf{12}$ (SON38) systems in the same experimental medium (30% w/w DMSO/water). **Figure 6** shows a change in the deprotonation profile of the ligand titration curve in the presence of copper. In fact, the curves for the systems containing copper lie below those of the ligand for a $\Delta > -1$, therefore pointing towards the formation of compounds with the deprotonated form of the ligand (CuL) and eventually copper ligand-hydroxide mixed complexes (CuLOH), in accordance with the complexation model presented in Table 5 and evidenced in **Figure 8b**. A ^1H NMR titration of the 1:1 $\text{Zn}^{2+}/\mathbf{12}$ (SON38) system in d_6 -DMSO/ D_2O medium was also performed in order to understand the coordination core. Notably, above $\text{pH} = 4.5$, a broadening of some peaks, namely those corresponding to methylene protons linked to the piperazine ring (protons 7 and 9-11, see **Figure 7**) was observed, while for the remaining peaks, corresponding to other protons of the molecule, the shape or chemical shift observed in the spectra of **12** (SON38) was kept. This observation can be interpreted in terms of higher magnetic anisotropy associated to the magnetic non-equivalence of each pair of these methylene protons of the complex species due to the increased rigidity of the piperazine ring, thus giving support to the hypothesis that the coordination of the copper ion involves both piperazine nitrogen atoms.

Evidence for identical coordination was already reported in the literature for some metal complexes with piperazine or 1,4-dimethylpiperazine, for which boat conformation was found [52,55,56]. Copper coordination involving the *N*-piperazine atoms was also established by X-ray crystallography for compounds with alkyl or aryl amines or heteroaromatic groups pending as arms from the two nitrogen atoms of piperazine [56–58].

Furthermore, ESI-MS data obtained for solutions of $\text{Cu}^{2+}/\mathbf{12}$, under 30% w/w DMSO/ H_2O medium, confirm the existence of a 1:1 copper complex as the species $[\text{CuLCl}]^+$ (see **Figure 9**).

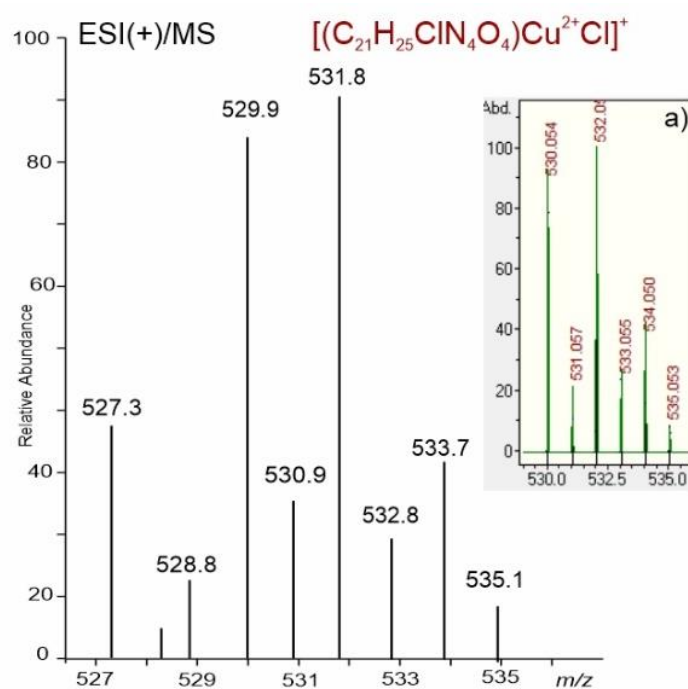


Figure 9. ESI-MS spectrum in positive mode of a solution of $\text{Cu}^{2+}/\mathbf{12}$ (**SON38**) 1:1 (pH= 5.68, $(C_L = 2.6 \times 10^{-4} \text{ M})$). The group of peaks at m/z 530/532 display an isotopic distribution pattern that agrees well with that calculated for $[\text{Cu}^{2+}(\text{C}_{21}\text{H}_{25}\text{ClN}_4\text{O}_4)\text{Cl}]^+$ as shown in insert a).

Finally, in the present study, difficulty in the accommodation of the metal ion in the coordination core of compound **12** (**SON38**) is reflected in the fact that the kinetics of formation of these copper complexes is slow, involving times of acquisition of each titration equilibrium point between 45-60 minutes for a > -1 . The steric hindrance involved in the formation of the copper complexes seems also evident from the low value of $p\text{Cu}$ (7.9) presented in Table 5, indicating that this kind of

hybrids has lower chelating capacity towards Cu^{2+} than other previously developed derivatives containing a stronger hydroxyl-phenylbenzimidazole chelating moiety ($\text{pCu} = 10.7\text{-}14.3$ [59,60]), but still valuable to be included in a multi-target design of molecules that can contrast the neurotoxicity due to metal dyshomeostasis in Alzheimer's disease.

Overall, the set of multi-target directed compounds presented herein appears as an innovative structural scaffold, showing ability to tackle multiple AD targets and also to potentially enforce synergic effects. Despite the existence of some limitations inherent to the multi-target strategy, since the design of the compounds must respect the time-course of the disease and the combination of selected targets must be effective for a given stage of the disease [61], the multi-target approach keeps being recognized as a good strategy to discover real disease modifying agents for such a complex disease.

Conclusions

In the present study, a series of donepezil-like hybrids were designed, synthesized and assayed against three different enzymes, AChE, BChE and FAAH. *In silico* studies were also performed to rationalize the obtained results. Compounds **1-10** include in their structure the benzylpiperidine moiety and resulted, in general, promising as potential multi-functional compounds. In particular, compound **10** showed the best results, due to its substantial good inhibitory activity within a small range (1.68-20.9 μM) considering all the enzymatic assays as well as to the interesting predicted ADME properties for CNS drugs. Moreover, it does not show significant cytotoxicity on SH-SY5Y and HepG2 at the higher concentration tested (100 μM) in a MTT assay.

Compounds **11-20** (piperazine series) showed a marked selectivity against AChE. In fact, compounds **12** (SON38) and **13** showed to be more active ($\text{IC}_{50} = 0.8$ and 2.8 nM, respectively) than

the parent compound donepezil, while having also additional ability to inhibit the innovative target FAAH and moderate/good potency against BChE (comparable with the commercial drug donepezil). QSAR study confirmed that the longer the spacer and the higher the number of polar atoms, the better is AChE inhibition. Docking studies also suggested that compound **12 (SON38)**, thanks to a particular conformation, has comparable ligand efficacy as acetylcholinesterase inhibitor considering donepezil as reference ligand; these modelling studies were also able to rationalize the considerable but less potent activity of the whole series **1-20** against BChE and FAAH. Compound **12 (SON38)** was also studied for its ability to chelate copper (II), confirming an interesting pharmacological profile ($pCu = 7.9$ at physiological pH) in the prevention of neurotoxicity due to metal dyshomeostasis and it does not show cytotoxicity in both cell lines studied in a MTT assay (SH-SY5Y and HepG2) even at very high concentrations (100 μ M).

. The obtained results allow to claim that **10** (as multi-functional ligand) and **12 (SON38)**, as highly potent AChE inhibitor and moderate copper chelator) may represent inspiring compounds for the development of future drugs with enlarged panel of targets for the treatment of Alzheimer's disease.

Experimental section

Chemistry

Reagents and solvents were purchased from common suppliers and were used without any further purification. Column chromatography was conducted using Geduran silica gel 60 A° (63–200 μ m) as a stationary phase. Mass spectrometry was conducted on a HP MS 6890-5973 MSD spectrometer, electron impact 70 eV, equipped with a HP ChemStation or with an Agilent LC–MS 1100 Series LC–MSD Trap System VL spectrometer, electrospray ionization (ESI). NMR spectra were recorded in the suitable deuterated solvent on Varian Mercury 300 NMR or Agilent VNMRS500 spectrometers. Chemical shifts (δ) are reported as parts per million (ppm) while the

coupling constants (J) in Hertz (Hz). NMR spectra of final compounds **1-20** are included in the supplementary material file (Figure S3). IR spectra were recorded on Perkin.Elmer 681 (Milan, Italy) spectrometer. For UPLC analyses, 10 μ L of the filtered solution were injected into an Agilent 1290 Infinity (AgilentTechnology, Inc., Wilmington, DE, USA) consisting of a binary pump (G4204A), an autosampler (G4226A) with a 10 μ L loop, a fluorescence detector (G1321B) fixed at 260nm (λ_{ex}) and 320nm (λ_{em}), a UV (DAD) detector (G4212A) set at $\lambda = 210$, $\lambda = 254$ and 260 nm λ and a software for Microsoft Windows 7 (Open LAB, CSD, Chemstation Edition). The separations were performed with an Eclipse XDB-C18 2.1 \times 150 mm Agilent analytical column, preceded by a 0.5 μ m pore size guard filter, with a column thermostat set at 30 $^{\circ}$ C (G1316C). The flow rate of mobile phase was set at 0.4 mL/min. Chromatographic separation was performed with a binary gradient of acetonitrile (ACN) in water that was used as mobile phase as follows: from 20% to 80% ACN in 8 min, then to 100% ACN for 3 min. The column was then brought to 20% ACN in 0.1 min and left to equilibrate for 3 min before the next run. Sample traces are included in the supplementary material file (Figure S4). For target compound **12 (SON38)**, elemental analysis was performed on a Fisons EA1108 CHNS/O instrument and was within the limit of $\pm 0.4\%$. Exact mass analyses of tested compounds were within the accepted values compared to the theoretical values. The purity of all tested compounds, on the basis of the panel of analyses performed, was estimated as $>95\%$. Melting points are uncorrected and were measured in open capillaries on a Gallenkamp electrothermal apparatus (Fisons Erba Science Ltd., Guildford, UK).

Preparation of ethyl phenoxy acetate derivatives 1b-7b and 8.1b.

General procedure.

Sodium ethoxide was prepared dissolving Na (1.696 mmol, 1 eq) in absolute ethanol (5 mL), then the suitable commercial phenol (1.696 mmol, 1 eq) was added and the solution was stirred for 30 minutes. Subsequently, a solution of ethyl bromoacetate (1.696 mmol, 1 eq) in absolute ethanol (5 mL), was added dropwise and the reaction mixture was refluxed for 23 h. The solvent was removed

in vacuo, and the resulting crude treated with diethyl ether (three times). The organic portions were collected and washed with 0.5 N NaOH and brine, dried over anhydrous Na₂SO₄, filtered and concentrated to dryness, affording the title compounds.

Ethyl 2-([1,1'-biphenyl]-4-yloxy)acetate (1b)

Starting from [1,1'-biphenyl]-4-ol, eluent: *n*-hexane/EtOAc 9:1. The title compound was obtained as a white solid, yield 62%. ¹H-NMR (300 MHz, CDCl₃) δ (ppm): 1.31 (t, J = 7.0 Hz, 3H, OCH₂CH₃), 4.29 (q, J = 7.0 Hz, 2H, OCH₂CH₃), 4.66 (s, 2H, OCH₂CO), 6.97 – 7.00 (m, 2H aromatics), 7.26 – 7.33 (m, 1H aromatic), 7.39 – 7.44 (m, 2H aromatics), 7.51 – 7.56 (m, 4H aromatics). GC-MS *m/z* (%): 256 (100) [M]⁺, 169 (49), 152 (62), 141 (24).

Ethyl 2-(4-chloro-2-nitrophenoxy)acetate (2b)

Starting from 4-chloro-2-nitrophenol. The compound was obtained as an orange solid, yield 81%. ¹H-NMR (500 MHz, CDCl₃) δ (ppm): 1.29 (t, J = 7.3 Hz, 3H, OCH₂CH₃), 4.26 (q, J = 7.3 Hz, 2H, OCH₂CH₃), 4.76 (s, 2H, OCH₂CO), 6.94 – 6.97 (m, 1H aromatic), 7.46 – 7.49 (m, 1H aromatic), 7.86 – 7.88 (m, 1H aromatic). GC-MS *m/z* (%): 261 (5) [M+2]⁺, 259 (12) [M]⁺, 187 (33), 185 (100), 158 (15), 156 (40).

Ethyl 2-(5-fluoro-2-nitrophenoxy)acetate (3b)

Starting from 5-fluoro-2-nitrophenol. The title compound was obtained as a yellow oil, yield 83%. ¹H-NMR (300 MHz, CDCl₃) δ (ppm): 1.30 (t, J = 7.1 Hz, 3H, OCH₂CH₃), 4.28 (q, J = 7.1 Hz, 2H, OCH₂CH₃), 4.77 (s, 2H, OCH₂CO), 6.63 – 6.71 (m, 1H aromatic), 6.73 – 6.84 (m, 1H aromatic), 7.95 – 8.01 (m, 1H aromatic). GC-MS *m/z* (%): 243 (7) [M]⁺, 197 (45), 169 (100), 124 (48).

Ethyl 2-(4-nitrophenoxy)acetate (4b)

Starting from 4-nitrophenol. The title compound was obtained as a white solid, yield 90%. ¹H-NMR (500 MHz, CDCl₃) δ (ppm): 1.31 (t, J = 7.3 Hz, 3H, OCH₂CH₃), 4.29 (q, J = 7.3 Hz, 2H, OCH₂CH₃), 4.71 (s, 2H, OCH₂CO), 6.96 – 7.00 (m, 2H aromatics), 8.20 – 8.23 (m, 2H aromatics). GC-MS *m/z* (%): 225 (98) [M]⁺, 152 (100), 122 (29), 76 (28).

Ethyl 2-(2-(trifluoromethyl)phenoxy)acetate (5b)

Starting from 2-(trifluoromethyl)phenol. The title compound was obtained as a colorless oil, yield 71%. ¹H-NMR (300 MHz, CDCl₃) δ (ppm): 1.28 (t, J = 7.1 Hz, 3H, OCH₂CH₃), 4.26 (q, J = 7.1 Hz, 2H, OCH₂CH₃), 4.72 (s, 2H, OCH₂CO), 6.84 – 6.91 (m, 1H aromatic), 7.01 – 7.10 (m, 1H aromatic), 7.42 – 7.51 (m, 1H aromatic), 7.57 – 7.63 (m, 1H aromatic). GC-MS *m/z* (%): 248 (3) [M]⁺, 220 (32), 205 (100).

Ethyl 2-(4-bromo-2,6-dimethylphenoxy)acetate (6b)

Starting from 4-bromo-2,6-dimethylphenol. The title compound was obtained as a colorless oil, yield 50%. ¹H-NMR (300 MHz, CDCl₃) δ (ppm): 1.33 (t, J = 6.9 Hz, 3H, OCH₂CH₃), 2.27 (s, 6H, PhCH₃), 4.28 (q, J = 6.9 Hz, 2H, OCH₂CH₃), 4.36 (s, 2H, OCH₂CO), 7.14 (s, 2H aromatics). GC-MS *m/z* (%): 288 (94) [M+2]⁺, 286 (95) [M]⁺, 215 (31), 213 (32), 201 (98), 199 (100), 185 (25), 183 (25), 91 (35).

Ethyl 2-(4-benzylphenoxy)acetate (7b)

Starting from 4-benzylphenol, eluent: *n*-hexane/EtOAc 9:1. The title compound was obtained as a colorless oil, yield 61%. ¹H NMR (300 MHz, CDCl₃) δ (ppm): 1.29 (t, J = 7 Hz, 3H, OCH₂CH₃), 3.92 (s, 2H, PhCH₂Ph), 4.26 (q, J = 7.0 Hz, 2H, OCH₂CH₃), 4.59 (s, 2H, OCH₂CO), 6.82 – 7.30 (m, 9H aromatics). GC-MS *m/z* (%): 270 (99) [M]⁺, 183 (100).

(E)-ethyl 2-(4-styrylphenoxy)acetate (8.Ib)

Starting from *trans*-4-styrylphenol, eluent: *n*-hexane/EtOAc 95:5. The title compound was obtained as a white solid, yield 73%. ¹H-NMR (300 MHz, CDCl₃) δ (ppm): 1.31 (t, 3H, OCH₂CH₃), 4.28 (q, 2H, OCH₂CH₃), 4.64 (s, 2H, OCH₂CO), 6.88 – 6.95 (m, 2H, aromatics), 6.98 (d, 1H, CH=CH), 7.07 (d, 1H, CH=CH), 7.21 – 7.50 (m, 7H, aromatics). GC-MS *m/z* (%): 282 (100) [M]⁺, 195 (35), 178 (36).

Preparation of ethyl 2-(4-phenethylphenoxy)acetate (8b)

A solution of (*E*)-ethyl 2-(4-styrylphenoxy)acetate (**8.1b**) (2.95 mmol, 17.35 eq) in THF (35 mL), was added to a stirred suspension of Wilkinson's catalyst (0.17 mmol, 1 eq) in absolute ethanol (30 mL). The reaction mixture was placed in an autoclave at 15 atm of H₂ pressure at room temperature for 48 h. The catalyst was removed via filtration over celite and the solvent was removed under vacuum. The crude was purified through chromatographic column (*n*-hexane/EtOAc 95:5), obtaining a white solid, yield 79%. ¹H NMR (300 MHz, CDCl₃) δ (ppm): 1.30 (t, J = 7.0 Hz 3H, OCH₂CH₃), 2.84 – 2.90 (m, 4H, PhCH₂CH₂Ph), 4.27 (q, J = 7.0 Hz, 2H, OCH₂CH₃), 4.60 (s, 2H, OCH₂CO), 6.80 – 7.30 (m, 9H aromatics), GC-MS *m/z* (%): 284 (15) [M]⁺, 193 (100), 107 (11).

Preparation of phenoxy acetic acid derivatives 1a-8a. General procedure

1 N NaOH (9.334 mmol, 10 eq) was added to a solution of the suitable ethyl phenoxy acetate derivatives (**1b-8b**) (0.993 mmol, 1 eq) in THF (10 mL). The mixture was stirred for 5 h at room temperature. Then, the organic solvent was removed under reduced pressure, the aqueous residue was acidified with 2 N HCl and then extracted with diethyl ether (three times). The collected organic portions were washed with brine, dried over anhydrous Na₂SO₄, filtered and concentrated to dryness, affording the title compounds.

2-([1,1'-Biphenyl]-4-yloxy)acetic acid (**1a**)

Starting from ethyl 2-([1,1'-biphenyl]-4-yloxy)acetate (**1b**). The title compound was obtained as a white solid, yield 96%; **m.p. = 190 – 192 °C**. ¹H-NMR (300 MHz, DMSO-d₆) δ (ppm): 4.11 (s, 2H, OCH₂CO), 6.86 – 6.90 (m, 2H aromatics), 7.26 – 7.61 (m, 7H aromatics). ESI-MS *m/z*: (IP: negative) 227 [M-H]⁻.

2-(4-Chloro-2-nitrophenoxy)acetic acid (**2a**)

Starting from ethyl 2-(4-chloro-2-nitrophenoxy)acetate (**2b**). The title compound was obtained as a yellow solid, yield 91%; **m.p. = 171 °C dec**. ¹H-NMR (500 MHz, DMSO) δ (ppm): 4.91 (s, 2H, OCH₂CO), 7.27 – 7.32 (m, 1H aromatic), 7.64 – 7.71 (m, 1H aromatic), 7.98 – 8.04 (m, 1H

aromatic), 13.28 (bs, 1H, COOH). ESI-MS m/z : (IP: negative) 232 $[M+2-H]^-$, 230 $[M-H]^-$; (IP: positive) 256 $[M+2+Na]^+$, 254 $[M+Na]^+$.

2-(5-Fluoro-2-nitrophenoxy)acetic acid (3a)

Starting from ethyl 2-(5-fluoro-2-nitrophenoxy)acetate (**3b**). The title compound was obtained as a beige solid, yield 89%; **m.p. = 158 °C dec.** 1H -NMR (300 MHz, DMSO) δ (ppm): 4.94 (s, 2H, OCH_2CO), 6.94 – 7.03 (m, 1H aromatic), 7.23 – 7.31 (m, 1H aromatic), 7.95 – 8.05 (m, 1H aromatic), 13.25 (bs, 1H, COOH). ESI-MS m/z : (IP: negative) 429 $[2M-H]^-$, 214 $[M-H]^-$; (IP: positive) 238 $[M+Na]^+$.

2-(4-Nitrophenoxy)acetic acid (4a)

Starting from ethyl 2-(4-nitrophenoxy)acetate (**4b**). The title compound was obtained as a yellow solid, yield 92%; **m.p. = 189 – 190 °C.** 1H -NMR (300 MHz, DMSO) δ (ppm): 4.85 (s, 2H, OCH_2CO), 7.09 – 7.13 (m, 2H aromatics), 8.15 – 8.20 (m, 2H aromatics). ESI-MS m/z : (IP: negative) 393 $[2M-H]^-$, 196 $[M-H]^-$; (IP: positive) 242 $[M+Na]^+$.

2-(2-(Trifluoromethyl)phenoxy)acetic acid (5a)

Starting from ethyl 2-(2-(trifluoromethyl)phenoxy)acetate (**5b**). The title compound was obtained as a white solid, yield 98%; **m.p. = 147 – 148 °C.** 1H -NMR (300 MHz, $CDCl_3$) δ (ppm): 4.75 (s, 2H, OCH_2CO), 6.88 – 6.94 (m, 1H aromatic), 7.04 – 7.14 (m, 1H aromatic), 7.46 – 7.54 (m, 1H aromatic), 7.59 – 7.64 (m, 1H aromatic). ESI-MS m/z : (IP: negative) 219 $[M-H]^-$; (IP: positive) 243 $[M+Na]^+$.

2-(4-Bromo-2,6-dimethylphenoxy)acetic acid (6a)

Starting from ethyl 2-(4-bromo-2,6-dimethylphenoxy)acetate (**6b**). The title compound was obtained as a white solid, yield 93%; **m.p. = 189 – 190 °C.** 1H -NMR (300 MHz, DMSO) δ (ppm): 2.29 (s, 6H, $PhCH_3$), 4.45 (s, 2H, OCH_2CO), 7.17 (s, 2H aromatics). ESI-MS m/z : (IP: positive) 283 $[M+2+Na]^+$, 281 $[M+Na]^+$.

2-(4-Benzylphenoxy)acetic acid (7a)

Starting from ethyl 2-(4-benzylphenoxy)acetate (**7b**). The title compound was obtained as a white solid, yield 98%; **m.p. = 117 – 118 °C**. ¹H NMR (300 MHz, CDCl₃) δ (ppm): 3.93 (s, 2H, PhCH₂Ph), 4.64 (s, 2H, OCH₂CO), 6.83 – 7.31 (m, 9H aromatics). GC-MS (methyl ester) m/z (%): 256 (89) [M]⁺, 183 (100), 165 (50), 152 (28).

2-(4-Phenethylphenoxy)acetic acid (8a)

Starting from ethyl 2-(4-phenethylphenoxy)acetate (**8b**). The title compound was obtained as a white solid, yield: 94%; **m.p. = 130 – 131 °C**. ¹H-NMR (300 MHz, CDCl₃) δ (ppm): 2.81 – 2.89 (m, 4H, PhCH₂CH₂Ph), 4.66 (s, 2H, OCH₂CO), 6.81 – 7.30 (m, 9H aromatics). GC-MS (methyl ester) m/z (%): 270 (12) [M]⁺, 179 (100).

Preparation of 2-(piperidin-4-ylmethyl)isoindoline-1,3-dione (21b)

Phthalic anhydride (8.8 mmol, 1 eq) and 4-(aminomethyl)piperidine (8.8 mmol, 1 eq) were heated at 160 °C for 4 h. The resulting dark brown solid was dissolved in 1 N HCl in absolute ethanol (6 mL), then the solvent was removed under vacuum. The compound was obtained as a white hydrochloride salt via crystallization with absolute ethanol, yield 25%; **m.p. = 214 °C dec**. ¹H-NMR (300 MHz, DMSO-d₆) δ (ppm): 1.37 – 1.46, 1.73 – 2.01 and 2.70 – 3.28 (m, 9H, piperidine), 3.47 (d, 2H, NCH₂CH), 7.83 – 7.91 (m, 4H aromatics). ESI-MS m/z: (IP: positive) 249 [M+H]⁺.

Preparation of 2-((1-benzylpiperidin-4-yl)methyl)isoindoline-1,3-dione (21a)

4-((1,3-dioxoisindolin-2-yl)methyl)piperidin-1-ium chloride (4.40 mmol, 1 eq) was dissolved in ethanol 96° (20 mL) and added with triethylamine (8.80 mmol, 2 eq) and benzyl bromide (4.40 mmol, 1eq). The reaction mixture was left at room temperature for 24 h, then the solvent was removed under reduced pressure. The residue was partitioned between CH₂Cl₂ and H₂O and the aqueous layer was extracted with CH₂Cl₂ (3 times). The collected organic layers were washed with brine, dried over anhydrous Na₂SO₄, filtered and concentrated under reduced pressure, obtaining a

yellow solid. The crude was purified by chromatography column (eluent EtOAc/MeOH 97:3), to give a white solid, yield 41%; m.p. 135 – 136 °C. ¹H-NMR (300 MHz, DMSO-d₆) δ (ppm): 1.07 – 1.15, 1.58 – 1.76 and 3.44 – 3.50 (m, 9H, piperidine), 2.73 (d, 2H, NCH₂CH), 3.41 (s, 2H, NCH₂Ph), 7.15 – 7.40 (m, 5H, aromatics, Ph-CH₂), 7.79 – 7.91 (m, 4H, phthalimide). ESI-MS m/z: (IP: positive) 335 [M+H]⁺.

Preparation of 2-(2-(4-Benzylpiperazin-1-yl)ethyl)isoindoline-1,3-dione (22a)

Phthalic anhydride (20.9 mmol, 1 eq) and 1-(2-aminoethyl)- piperazine (20.9 mmol, 1 eq) were heated at 160 °C for 4 h. The resulting dark brown oil **22b** (2-(2-(piperazin-1-yl)ethyl)isoindoline-1,3-dione, 20.9 mmol, 1 eq) was dissolved in ethanol 96° (46 mL) and added with KOH (25.1 mmol, 1.2 eq) and benzyl bromide (20.9 mmol, 1 eq). The reaction mixture was stirred at room temperature for 24 h, then the solvent was removed in vacuo. The residue was partitioned between diethyl ether and H₂O and the aqueous layer was extracted with diethyl ether (three times). The collected organic portions were washed with brine, dried over anhydrous Na₂SO₄, filtered and concentrated to dryness, obtaining a yellow solid. The crude was purified by chromatography column (eluent *n*-hexane/EtOAc 8:2), to give a white solid, yield 47%; m.p. 88 – 90 °C. ¹H-NMR (400 MHz, CDCl₃) δ (ppm): 2.39 – 2.52 (m, 8H, piperazine), 2.60 (t, 2H, J = 6.7 Hz, phthalimide-CH₂CH₂N), 3.44 (s, 2H, NCH₂Ph), 3.78 (t, 2H, J = 6.7 Hz, phthalimide-CH₂CH₂N), 7.19 – 7.27 (m, 5H, aromatics, Ph-CH₂), 7.67 – 7.69 and 7.80 – 7.82 (m, 4H, phthalimide). ESI-MS m/z: (IP: positive) 350 [M+H]⁺.

Preparation of compounds 21 and 22

2-((1-Benzylpiperidin-4-yl)methyl)isoindoline-1,3-dione (**21a**) or 2-(2-(4-benzylpiperazin-1-yl)ethyl)-isoindoline-1,3-dione (**22a**) (1.02 mmol) was dissolved in an aqueous solution of MeNH₂ 40% (w/w, 9 mL). Then, the mixture was stirred at room temperature for 72 h. Subsequently, an aqueous solution of 20% (w/w) NaOH (14 mL) was added and the resulting mixture was stirred for 2 h. Then, NaCl (18 mmol) was added and the solution was extracted with CH₂Cl₂ (three times).

The collected organic layers were washed with water, dried over anhydrous Na₂SO₄, filtered and concentrated to dryness, affording the title compounds.

(1-Benzylpiperidin-4-yl)methanamine (21)

Starting from 2-((1-benzylpiperidin-4-yl)methyl)isoindoline-1,3-dione (**21a**). The title compound was obtained as a yellow oil, yield 91%. ¹H-NMR (300 MHz, DMSO-d₆) δ (ppm): 1.00 – 1.23, 1.82 – 1.89 and 2.37 – 2.39 (m, 9H, piperidine), 2.77 (d, 2H, J = 11.5 Hz, NCH₂CH), 3.41 (s, 2H, NCH₂Ph), 7.20 – 7.33 (m, 5H, aromatics, Ph-CH₂). ESI-MS m/z: (IP: positive) 205 [M+H]⁺.

2-(4-Benzyl-1-piperazine-1-yl)ethanamine (22)

Starting from 2-(2-(4-benzylpiperazin-1-yl)ethyl)isoindoline-1,3-dione (**22a**). The title compound was obtained as a yellow oil, yield 99%. ¹H NMR (400 MHz, CDCl₃) δ (ppm): 2.35 – 2.43 (m, 10H, 8H piperazine + 2H NH₂CH₂CH₂N), 2.73 (t, 2H, J = 6.1 Hz, NH₂CH₂CH₂N), 3.46 (s, 2H, NCH₂Ph), 7.19 – 7.27 (m, 5H, aromatics, Ph-CH₂). ESI-MS m/z: (IP: positive) 220 [M+H]⁺.

Preparation of the final compounds (1-20).

General procedure.

The suitable phenoxy acetic acid derivatives **1a-10a** (0.79 mmol, 3 eq), 1-hydroxybenzotriazole hydrate (HOBt, 0.263 mmol, 1 eq) and *N,N'*-diisopropylcarbodiimide (DIC, 1.048 mmol, 4 eq), were added to a solution of (1-benzylpiperidin-4-yl)methanamine (**21**) or 2-(4-benzyl-1-piperazine-1-yl)ethanamine (**22**) (0.524 mmol, 2 eq) in CH₂Cl₂ (5 mL). The mixture was stirred for 16 h at room temperature. Then, it was filtered through a Büchner funnel, and the obtained solution was washed with 0.5 N NaOH and brine. The organic portion was dried over anhydrous Na₂SO₄, filtered and concentrated at reduced pressure. The crude product was purified through column chromatography.

2-([1,1'-Biphenyl]-4-yloxy)-N-((1-benzylpiperidin-4-yl)methyl)acetamide (1)

Starting from 2-([1,1'-biphenyl]-4-yloxy)acetic acid (**1a**) and (1-benzylpiperidin-4-yl)methanamine (**21**), eluent: 100% EtOAc. The title compound was obtained as a white solid, yield 45%; **m.p. = 149–150 °C**. ¹H-NMR (300 MHz, CDCl₃) δ (ppm): 1.23–1.38, 1.47–1.74, 1.86–1.98 and 2.82–2.94 (m, 9H, piperidine), 3.25 (t, *J* = 6.4 Hz, 2H, NHCH₂CH), 3.49 (s, 2H, NCH₂Ph), 4.54 (s, 2H, OCH₂CO), 6.59–6.61 (bs, 1H, NH), 6.93–7.05 (m, 2H aromatics), 7.21–7.47 (m, 8H aromatics), 7.49–7.61 (m, 4H aromatics). ¹³C NMR (126 MHz, CDCl₃) δ (ppm): 29.86, 36.08, 44.49, 53.21, 63.26, 67.55, 114.97, 126.77, 126.94, 126.99, 128.13, 128.44, 128.77, 129.14, 135.33, 138.28, 140.32, 156.67, 168.12. UPLC: t_R = 13.3 min; HRMS (C₂₇H₃₀N₂O₂+H⁺): calculated 415.2380 found 415.2383.

N-((1-Benzylpiperidin-4-yl)methyl)-2-(4-chloro-2-nitrophenoxy)acetamide (2)

Starting from 2-(4-chloro-2-nitrophenoxy)acetic acid (**2a**) and (1-benzylpiperidin-4-yl)methanamine (**21**), eluent: CH₂Cl₂/MeOH 95:5, then 100% EtOAc. The title compound was obtained as a yellow solid, yield 25%; **m.p. = 105–106 °C**. ¹H-NMR (500 MHz, CDCl₃) δ (ppm): 1.30–1.39, 1.51–1.74, 1.92–2.00 and 2.87–2.94 (m, 9H, piperidine), 3.28 (t, *J* = 6.4 Hz, 2H, NHCH₂CH), 3.49 (s, 2H, NCH₂Ph), 4.60 (s, 2H, OCH₂CO), 6.98–7.03 (m, 1H aromatic), 7.16–7.21 (m, 1H, NH), 7.21–7.32 (m, 5H aromatics), 7.55–7.60 (m, 1H aromatic), 8.02–8.04 (m, 1H aromatic). ¹³C NMR (126 MHz, CDCl₃) δ (ppm): 29.86, 36.06, 44.68, 53.22, 63.26, 68.01, 115.88, 126.49, 126.90, 126.96, 128.12, 129.11, 135.11, 138.39, 138.94, 149.60, 166.11. UPLC: t_R = 12.9 min; HRMS (C₂₁H₂₄ClN₃O₄+H⁺): calculated 418.1528 found 418.1533.

N-((1-Benzylpiperidin-4-yl)methyl)-2-(5-fluoro-2-nitrophenoxy)acetamide (3)

Starting from 2-(5-fluoro-2-nitrophenoxy)acetic acid (**3a**) and (1-benzylpiperidin-4-yl)methanamine (**21**), eluent: 100% EtOAc. The title compound was obtained as a yellow solid, yield 36%; **m.p. = 92–93 °C**. ¹H-NMR (300 MHz, CDCl₃) δ (ppm): 1.27–1.42, 1.50–1.78, 1.90–2.02 and 2.85–2.94

(m, 9H, piperidine), 3.29 (t, $J = 6.3$ Hz, 2H, NHCH_2CH), 3.49 (s, 2H, NCH_2Ph), 4.58 (s, 2H, OCH_2CO), 6.71 – 6.88 (m, 2H aromatics), 7.19 – 7.34 (m, 6H, 5H aromatics + 1H NH), 8.11 – 8.18 (m, 1H aromatic). ^{13}C NMR (126 MHz, CDCl_3) δ (ppm): 29.89, 36.08, 44.71, 53.24, 63.28, 67.94, 102.56 (d, $J_{2, \text{C-F}} = 26$ Hz) 108.93 (d, $J_{2, \text{C-F}} = 26$ Hz), 126.88, 128.11, 129.09, 129.18, 135.17, 138.46, 153.01 (d, $J_{3, \text{C-F}} = 11.3$ Hz), 165.88, 166.19 (d, $J_{1, \text{C-F}} = 260$ Hz). UPLC: $t_{\text{R}} = 8.8$ min; HRMS ($\text{C}_{21}\text{H}_{24}\text{FN}_3\text{O}_4 + \text{H}^+$): calculated 402.1824 found 402.1825.

N-((1-Benzylpiperidin-4-yl)methyl)-2-(4-nitrophenoxy)acetamide (4)

Starting from 2-(4-nitrophenoxy)acetic acid (**4a**) and (1-benzylpiperidin-4-yl)methanamine (**21**), eluent: $\text{CH}_2\text{Cl}_2/\text{MeOH}$ 97:3, then 100% EtOAc. The title compound was obtained as a yellow solid, yield 17%; m.p. = 106 – 108 °C. ^1H -NMR (300 MHz, CDCl_3) δ (ppm): 1.22 – 1.38, 1.47 – 1.67, 1.86 – 2.00 and 2.83 – 2.93 (m, 9H, piperidine), 3.26 (t, $J = 6.3$ Hz, 2H, NHCH_2CH), 3.48 (s, 2H, NCH_2Ph), 4.58 (s, 2H, OCH_2CO), 6.47–6.57 (bs, 1H, NH), 6.97 – 7.05 (m, 2H aromatics), 7.21 – 7.34 (m, 5H aromatics), 8.21 – 8.28 (m, 2H aromatics). ^{13}C NMR (126 MHz, CDCl_3) δ (ppm): 29.86, 36.03, 44.60, 53.15, 63.25, 67.65, 114.79, 126.09, 126.97, 128.15, 129.12, 138.22, 142.61, 161.72, 166.65. UPLC: $t_{\text{R}} = 5.2$ min; HRMS ($\text{C}_{21}\text{H}_{25}\text{N}_3\text{O}_4 + \text{H}^+$): calculated 384.1918 found 384.1923.

N-((1-Benzylpiperidin-4-yl)methyl)-2-(2-(trifluoromethyl)phenoxy)acetamide (5)

Starting from 2-(2-(trifluoromethyl)phenoxy)acetic acid (**5a**) and (1-benzylpiperidin-4-yl)methanamine (**21**), eluent: 100% EtOAc. The title compound was obtained as a white solid, yield 17%; m.p. = 121 – 122 °C. ^1H -NMR (500 MHz, CDCl_3) δ (ppm): 1.24 – 1.37, 1.47 – 1.54, 1.63 – 1.70, 1.92 – 1.99 and 2.85 – 2.92 (m, 9H, piperidine), 3.26 (t, $J = 6.4$ Hz, 2H, NHCH_2CH), 3.49 (s, 2H, NCH_2Ph), 4.55 (s, 2H, OCH_2CO), 6.74 – 6.79 (bs, 1H, NH), 6.94 – 6.98 (m, 1H aromatic), 7.08 – 7.13 (m, 1H aromatic), 7.22 – 7.25 (m, 2H aromatic), 7.27 – 7.33 (m, 3H aromatics), 7.50 – 7.56 (m, 1H aromatic), 7.59 – 7.64 (m, 1H aromatic). ^{13}C NMR (126 MHz, CDCl_3) δ (ppm): 29.80, 36.03, 44.57, 53.24, 63.27, 67.27, 112.82, 118.74 (q, $J_{2, \text{C-F}} = 31.5$ Hz), 121.48, 123.70 (q, $J_{1, \text{C-F}} =$

273.4 Hz), 126.87, 127.35 (q, $J_{3, C-F} = 5.1$ Hz), 128.12, 129.05, 133.76, 138.55, 154.65, 166.98.

UPLC: $t_R = 5.2$ min; HRMS ($C_{22}H_{25}F_3N_2O_2+H^+$): calculated 407.1941 found 407.1945.

N-((1-Benzylpiperidin-4-yl)methyl)-2-(4-bromo-2,6-dimethylphenoxy)acetamide (6)

Starting from 2-(4-bromo-2,6-dimethylphenoxy)acetic acid (**6a**) and (1-benzylpiperidin-4-yl)methanamine (**21**), eluent: $CH_2Cl_2/MeOH$ 97:3, then 100% EtOAc. The title compound was obtained as a white solid, yield 8%; m.p. = 143 – 144 °C. 1H -NMR (300 MHz, $CDCl_3$) δ (ppm): 1.30 – 1.43, 1.59 – 1.75, 1.92 – 2.03 and 2.87 – 2.95 (m, 9H, piperidine), 2.21 (s, 6H, $PhCH_3$), 3.29 (t, $J = 6.4$ Hz, 2H, $NHCH_2CH$), 3.50 (s, 2H, NCH_2Ph), 4.23 (s, 2H, OCH_2CO), 6.86–6.96 (bs, 1H, NH), 7.15–7.17 (m, 2H aromatics), 7.27 – 7.36 (m, 5H aromatics). ^{13}C NMR (126 MHz, $CDCl_3$) δ (ppm): 16.06, 29.97, 35.98, 44.52, 53.22, 63.27, 70.51, 117.39, 126.95, 128.14, 129.11, 131.77, 132.59, 138.34, 153.38, 168.24. UPLC: $t_R = 8.8$ min; HRMS ($C_{23}H_{29}BrN_2O_2+H^+$): calculated 445.1485 found 445.1483.

2-(4-Benzylphenoxy)-N-((1-benzylpiperidin-4-yl)methyl)acetamide (7)

Starting from 2-(4-benzylphenoxy)acetic acid (**7a**) and (1-benzylpiperidin-4-yl)methanamine (**21**), eluent: 100% EtOAc. The title compound was obtained as a white solid, yield 12%; m.p. = 114 °C dec. 1H -NMR (500 MHz, $CDCl_3$) δ (ppm): 1.30 – 1.40, 1.50 – 1.67, 1.97 – 2.06 and 2.92 – 2.99 (m, 9H, piperidine), 3.22 (t, $J = 6.5$ Hz, 2H, $NHCH_2CH$), 3.58 (s, 2H, NCH_2Ph), 3.91 (s, 2H, $PhCH_2Ph$), 4.46 (s, 2H, OCH_2CO), 6.61–6.68 (bs, 1H, NH), 6.80 – 6.85 (m, 2H aromatics), 7.08 – 7.22 (m, 5H aromatics), 7.23 – 7.36 (m, 7H aromatics). ^{13}C NMR (126 MHz, $CDCl_3$) δ (ppm): 29.59, 35.87, 40.99, 44.38, 53.00, 63.01, 67.51, 114.67, 126.09, 127.13, 128.20, 128.47, 128.75, 129.30, 130.15, 134.93, 137.65, 141.14, 155.57, 168.34. UPLC: $t_R = 6.6$ min; HRMS ($C_{28}H_{32}N_2O_2+H^+$): calculated 429.2537 found 429.2542.

N-((1-Benzylpiperidin-4-yl)methyl)-2-(4-phenethylphenoxy)acetamide (8)

Starting from 2-(4-phenethylphenoxy)acetic acid (**8a**) and (1-benzylpiperidin-4-yl)methanamine (**21**), eluent: 100% EtOAc. The title compound was obtained as a white solid, yield 52%; **m.p.** = 112 – 113 °C. ¹H-NMR (300 MHz, CDCl₃) δ (ppm): 1.20 – 1.36, 1.58 – 1.66 and 1.87 – 1.98 (m, 7H piperidine), 2.83 – 2.90 (m, 6H, 4H PhCH₂CH₂Ph + 2H piperidine), 3.23 (t, J = 6.4 Hz, 2H, NHCH₂CH), 3.48 (s, 2H, NCH₂Ph), 4.47 (s, 2H, OCH₂CO), 6.60–6.68 (bs, 1H, NH), 6.79 – 6.85 (m, 2H aromatics), 7.07 – 7.32 (m, 12H aromatics). ¹³C NMR (126 MHz, CDCl₃) δ (ppm): 29.91, 36.09, 36.94, 38.03, 44.46, 53.25, 63.31, 67.56, 114.54, 125.93, 126.91, 128.13, 128.31, 128.43, 129.10, 129.67, 135.49, 138.43, 141.54, 155.47, 168.33. UPLC: t_R = 5.2 min; HRMS (C₂₉H₃₄N₂O₂+H⁺): calculated 443.2693 found 443.2697.

N-((1-Benzylpiperidin-4-yl)methyl)-2-(4-methoxyphenoxy)acetamide (9)

Starting from 2-(4-methoxyphenoxy)acetic acid (**9a**) and (1-benzylpiperidin-4-yl)methanamine (**21**), eluent: CH₂Cl₂/MeOH 97:3, then 100% EtOAc. The title compound was obtained as a white solid, yield 19%; **m.p.** = 93 – 94 °C. ¹H-NMR (500 MHz, CDCl₃) δ (ppm): 1.22 – 1.34, 1.47 – 1.58, 1.60 – 1.63, 1.88 – 1.98 and 2.83 – 2.91 (m, 9H, piperidine), 3.23 (t, J = 6.5 Hz, 2H, NHCH₂CH), 3.48 (s, 2H, NCH₂Ph), 3.77 (s, 3H, OCH₃), 4.43 (s, 2H, OCH₂CO), 6.60–6.67 (bs, 1H, NH), 6.81–6.88 (m, 4H aromatics), 7.21 – 7.33 (m, 5H aromatics). ¹³C NMR (126 MHz, CDCl₃) δ (ppm): 29.67, 36.00, 44.41, 53.17, 55.69, 63.20, 68.22, 114.86, 115.68, 127.00, 128.15, 129.18, 151.32, 154.77, 168.47. UPLC: t_R = 6.9 min; HRMS (C₂₂H₂₈N₂O₃+H⁺) calculated 369.2173 found 369.2175.

N-((1-Benzylpiperidin-4-yl)methyl)-2-(4-chlorophenoxy)acetamide (10)

Starting from 2-(4-chlorophenoxy)acetic acid (**10a**) and (1-benzylpiperidin-4-yl)methanamine (**21**), eluent: CH₂Cl₂/MeOH 97:3, then 100% EtOAc. The title compound was obtained as a white solid, yield 22%; **m.p.** = 96 – 97 °C. ¹H-NMR (500 MHz, CDCl₃) δ (ppm): 1.24 – 1.33, 1.48 – 1.66, 1.90 – 1.96 and 2.85 – 2.90 (m, 9H, piperidine), 3.24 (t, J = 6.5 Hz, 2H, NHCH₂CH), 3.48 (s, 2H, NCH₂Ph), 4.46 (s, 2H, OCH₂CO), 6.56 – 6.59 (bs, 1H, NH), 6.82 – 6.87 (m, 2H aromatics), 7.22 –

7.33 (m, 7H aromatics). FT-IR (vaselin oil, wavenumber) cm^{-1} : 3244 (NH, s, amide), 1658 (CO, s, amide I), 1518 (NH, s, amide II). ^{13}C NMR (126 MHz, CDCl_3) δ (ppm): 29.89, 36.06, 44.49, 53.21, 63.29, 67.67, 115.97, 126.92, 127.19, 128.13, 129.11, 129.69, 138.36, 155.74, 167.72. UPLC: t_{R} = 5.2 min; HRMS ($\text{C}_{21}\text{H}_{25}\text{ClN}_2\text{O}_2+\text{H}^+$) calculated 373.1677 found 373.1682.

2-([1,1'-Biphenyl]-4-yloxy)-N-(2-(4-benzylpiperazin-1-yl)ethyl)acetamide (11)

Starting from 2-([1,1'-biphenyl]-4-yloxy)acetic acid (**1a**) and 2-(4-benzyl-1-piperazine-1-yl)ethanamine (**22**), eluent: $\text{CH}_2\text{Cl}_2/\text{MeOH}$ 98:2. The title compound was obtained as a white solid, yield 42%; m.p. = 127 °C dec. ^1H -NMR (300 MHz, CDCl_3) δ (ppm): 2.25 – 2.53 (m, 10H, 2H CH_2CH_2 piperazine + 8 H piperazine), 3.41 (q, J = 5.8 Hz, 2H, NHCH_2CH_2), 3.46 (s, 2H, Piperazine CH_2Ph), 4.55 (s, 2H, OCH_2CO), 6.96 – 7.02 (m, 2H aromatics), 7.13 – 7.20 (bs, 1H, NH), 7.22 – 7.36 (m, 6H aromatics), 7.39 – 7.47 (m, 2H aromatics), 7.51 – 7.59 (m, 4H aromatics). ^{13}C NMR (126 MHz, CDCl_3) δ (ppm): 35.51, 52.68, 53.07, 55.98, 63.01, 67.50, 114.92, 126.73, 126.97, 127.01, 128.17, 128.39, 128.80, 129.13, 135.13, 138.01, 140.36, 156.86, 168.05. UPLC: t_{R} = 6.0 min; HRMS ($\text{C}_{27}\text{H}_{30}\text{N}_3\text{O}_2+\text{H}^+$): calculated 430.2489, found 430.2503.

N-(2-(4-Benzylpiperazin-1-yl)ethyl)-2-(4-chloro-2-nitrophenoxy)acetamide (12)

Starting from 2-(4-chloro-2-nitrophenoxy)acetic acid (**2a**) and 2-(4-benzyl-1-piperazine-1-yl)ethanamine (**22**), eluent: $\text{CH}_2\text{Cl}_2/\text{MeOH}$ 9:1, then 100% EtOAc. The title compound was obtained as a white solid, yield 8%; m.p. = 109 – 110 °C. ^1H -NMR (300 MHz, CDCl_3) δ (ppm): 2.36 – 2.65 (m, 10H, 2H CH_2CH_2 piperazine + 8H piperazine), 3.44 (q, J = 5.4 Hz, 2H, NHCH_2CH_2), 3.55 (s, 2H, piperazine CH_2Ph), 4.60 (s, 2H, OCH_2CO), 6.96 – 7.04 (m, 1H aromatic), 7.17 – 7.44 (m, 6H, 5H aromatics + 1H NH), 7.53 – 7.60 (m, 1H aromatic), 7.95 – 8.01 (m, 1H aromatic). ^{13}C NMR (126 MHz, CDCl_3) δ (ppm): 35.94, 52.87, 56.23, 62.99, 68.01, 115.70, 126.24, 126.80, 126.95, 128.15, 129.21, 134.67, 138.21, 139.36, 149.45, 166.05. Analysis calc. for $\text{C}_{21}\text{H}_{25}\text{ClN}_4\text{O}_4 \cdot 0.5\text{H}_2\text{O}$: C 57.08, H 5.93, N 12.68 %; found: C 56.99, H 6.16, N 12.74 %. FT-IR (vaselin oil, wavenumber) cm^{-1} : 3376 (NH, s, amide), 1671 (CO, s, amide I), 1609 (m, NO_2), 1520

(NH, s, amide II), 1344 (m, NO₂). UPLC: t_R = 8.6 min; HRMS (C₂₁H₂₅ClN₄O₄+Na⁺): calculated 455.1457 found 455.1454.

N-(2-(4-Benzylpiperazin-1-yl)ethyl)-2-(5-fluoro-2-nitrophenoxy)acetamide (**13**)

Starting from 2-(5-fluoro-2-nitrophenoxy)acetic acid (**3a**) and 2-(4-benzyl-1-piperazine-1-yl)ethanamine (**22**), eluent: 100% EtOAc. The title compound was obtained as a white solid, yield 60%; m.p.=116 °C dec. ¹H-NMR (300 MHz, CDCl₃) δ (ppm): 2.38 – 2.67 (m, 10H, 2H CH₂CH₂ piperazine + 8H piperazine), 3.46 (q, J = 5.7 Hz, 2H, NHCH₂CH₂), 3.54 (s, 2H, piperazine CH₂Ph), 4.58 (s, 2H, OCH₂CO), 6.72 – 6.88 (m, 2H aromatics), 7.21 – 7.37 (m, 5H aromatics), 7.40 – 7.52 (bs, 1H, NH), 8.06 – 8.15 (m, 1H aromatic). ¹³C NMR (126 MHz, CDCl₃) δ (ppm): 36.02, 52.88, 52.91, 56.30, 62.99, 67.96, 102.47 (d, J_{2, C-F} = 27.7 Hz), 108.74, (d, J_{2, C-F} = 22.7 Hz), 126.93, 128.14, 128.83 (d, J_{3, C-F} = 11.3 Hz), 129.19, 135.52, 138.27, 152.90 (d, J_{3, C-F} = 11.3 Hz), 165.81, 165.95 (d, J_{1, C-F} = 260 Hz). FT-IR (vaselin oil, wavenumber) cm⁻¹: 3358 (NH, s, amide), 1676 (CO, s, amide I), 1622 (m, NO₂), 1521 (NH, s, amide II), 1344 (m, NO₂). UPLC: t_R = 6.1 min; HRMS (C₂₁H₂₅FN₄O₄+Na⁺): calculated 439.1752 found 439.1756.

N-(2-(4-Benzylpiperazin-1-yl)ethyl)-2-(4-nitrophenoxy)acetamide (**14**)

Starting from 2-(4-nitrophenoxy)acetic acid (**4a**) and 2-(4-benzyl-1-piperazine-1-yl)ethanamine (**22**), eluent: CH₂Cl₂/MeOH 9:1. The title compound was obtained as a white solid, yield 40%; m.p. = 70 – 72 °C. ¹H-NMR (500 MHz, CDCl₃) δ (ppm): 2.30 – 2.57 (m, 10H, 2H CH₂CH₂piperazine + 8H piperazine), 3.41 (q, J = 5.6 Hz, 2H, NHCH₂CH₂), 3.50 (s, 2H, piperazineCH₂Ph), 4.59 (s, 2H, OCH₂CO), 6.95 – 7.04 (m, 2H aromatics), 7.06 – 7.16 (bs, 1H, NH), 7.19 – 7.38 (m, 5H aromatics), 8.21 – 8.29 (m, 2H aromatics). ¹³C NMR (126 MHz, CDCl₃) δ (ppm): 35.50, 52.68, 53.02, 55.90, 62.98, 67.63, 114.75, 126.08, 127.10, 128.21, 129.16, 137.74, 142.48, 161.96, 166.57. UPLC: t_R = 5.2 min; HRMS (C₂₁H₂₆N₄O₄+H⁺): calculated 399.2027 found 399.2030.

N-(2-(4-Benzylpiperazin-1-yl)ethyl)-2-(2-(trifluoromethyl)phenoxy)acetamide (**15**)

Starting from 2-(2-(trifluoromethyl)phenoxy)acetic acid (**5a**) and 2-(4-benzyl-1-piperazine-1-yl)ethanamine (**22**), eluent: 100% EtOAc. The title compound was obtained as a colorless oil, yield 36%. ¹H-NMR (300 MHz, CDCl₃) δ (ppm): 2.33 – 2.64 (m, 10H, 2H CH₂CH₂piperazine + 8H piperazine), 3.39 – 3.55 (m, 4H, 2H NHCH₂CH₂ + 2H piperazineCH₂Ph), 4.56 (s, 2H, OCH₂CO), 6.92 – 7.00 (m, 1H aromatic), 7.06 – 7.14 (m, 1H aromatic), 7.19 – 7.35 (m, 6H, 5H aromatics + 1H NH), 7.48 – 7.57 (m, 1H aromatic), 7.60 – 7.66 (m, 1H aromatic). ¹³C NMR (126 MHz, CDCl₃) δ (ppm): 35.74, 52.75, 52.80, 56.22, 63.03, 67.32, 112.74, 118.88 (q, J_{2, C-F} = 30.2 Hz), 121.32, 123.66 (q, J_{1, C-F} = 273.4 Hz), 126.98, 127.29 (q, J_{3, C-F} = 5.0 Hz), 128.16, 129.16, 133.63, 138.17, 154.83, 167.00. UPLC: t_R = 6.8 min; HRMS (C₂₂H₂₆F₃N₃O₂+H⁺): calculated 422.2050 found 422.2066.

N-(2-(4-Benzylpiperazin-1-yl)ethyl)-2-(4-bromo-2,6-dimethylphenoxy)acetamide (**16**)

Starting from 2-(4-bromo-2,6-dimethylphenoxy)acetic acid (**6a**) and 2-(4-benzyl-1-piperazine-1-yl)ethanamine (**22**), eluent: CH₂Cl₂/MeOH 9:1, then 100% EtOAc. The title compound was obtained as a colorless oil, yield 58%. ¹H-NMR (300 MHz, CDCl₃) δ (ppm): 2.23 (s, 6H, PhCH₃), 2.40 – 2.69 (m, 10H, 2H CH₂CH₂ piperazine + 8H piperazine), 3.42 – 3.56 (m, 4H, 2H NHCH₂CH₂ + 2H piperazineCH₂Ph), 4.25 (s, 2H, OCH₂CO), 7.16 – 7.38 (m, 8H, 6H aromatics + 1H NH). ¹³C NMR (126 MHz, CDCl₃) δ (ppm): 16.28, 35.60, 52.86, 53.02, 56.39, 62.96, 70.71, 117.23, 127.06, 128.19, 129.15, 131.72, 132.64, 137.91, 153.85, 168.21. UPLC: t_R = 7.7 min; HRMS (C₂₃H₃₀BrN₃O₂+H⁺): calculated 460.1594 found 460.1595.

2-(4-Benzylphenoxy)-*N*-(2-(4-benzylpiperazin-1-yl)ethyl)acetamide (**17**)

Starting from 2-(4-benzylphenoxy)acetic acid (**7a**) and 2-(4-benzyl-1-piperazine-1-yl)ethanamine (**22**), eluent: 100% EtOAc. The title compound was obtained as a white solid, yield 55%; m.p. = 81 – 82 °C. ¹H-NMR (500 MHz, CDCl₃) δ (ppm): 2.22 – 2.60 (m, 10H, 2H CH₂CH₂ piperazine + 8H piperazine), 3.38 (q, J = 5.8 Hz, 2H, NHCH₂CH₂), 3.47 (s, 2H, piperazineCH₂Ph), 3.93 (s, 2H, PhCH₂Ph), 4.47 (s, 2H, OCH₂CO), 6.81 – 6.86 (m, 2H aromatics), 7.10 – 7.22 (m, 6H, 5H aromatics + 1H NH), 7.23 – 7.34 (m, 7H aromatics). ¹³C NMR (126 MHz, CDCl₃) δ (ppm): 35.47,

41.04, 52.68, 53.04, 56.09, 62.98, 67.50, 114.66, 126.10, 127.06, 128.20, 128.47, 128.76, 129.16, 130.09, 134.76, 137.97, 141.18, 155.74, 168.20. UPLC: $t_R = 6.4$ min; HRMS ($C_{28}H_{33}N_3O_2+H^+$): calculated 444.2646 found 444.2650.

N-(2-(4-Benzylpiperazin-1-yl)ethyl)-2-(4-phenethylphenoxy)acetamide (**18**)

Starting from 2-(4-phenethylphenoxy)acetic acid (**8a**) and 2-(4-benzyl-1-piperazine-1-yl)ethanamine (**22**), eluent: 100% EtOAc. The title compound was obtained as a white solid, yield 34%; m.p. = 91 – 92 °C. 1H -NMR (500 MHz, $CDCl_3$) δ (ppm): 2.26 – 2.52 (m, 10H, 2H CH_2CH_2 piperazine + 8H piperazine), 2.88 (s, 4H, $PhCH_2CH_2Ph$), 3.40 (q, $J = 5.8$ Hz, 2H, $NHCH_2CH_2$), 3.49 (s, 2H, piperazine CH_2Ph), 4.47 (s, 2H, OCH_2CO), 6.81 – 6.85 (m, 2H aromatics), 7.09 – 7.13 (m, 2H aromatics), 7.14 – 7.22 (m, 4H aromatics), 7.23 – 7.33 (m, 7H, 6H aromatics + 1H NH). ^{13}C NMR (126 MHz, $CDCl_3$) δ (ppm): 35.50, 36.93, 38.04, 52.71, 53.09, 56.10, 63.02, 67.53, 114.53, 125.93, 127.05, 128.20, 128.31, 128.42, 129.14, 129.63, 135.30, 138.02, 141.54, 155.63, 168.25. FT-IR (vaselin oil, wavenumber) cm^{-1} : 3399 (NH, s, amide), 1661 (CO, s, amide I), 1526 (NH, s, amide II). UPLC: $t_R = 8.7$ min; HRMS ($C_{29}H_{35}N_3O_2+H^+$): calculated 458.2802 found 458.2803.

N-(2-(4-Benzylpiperazin-1-yl)ethyl)-2-(4-methoxyphenoxy)acetamide (**19**)

Starting from 2-(4-methoxyphenoxy)acetic acid (**9a**) and 2-(4-benzyl-1-piperazine-1-yl)ethanamine (**22**), eluent: $CH_2Cl_2/MeOH$ 95:5, then 100% EtOAc. The title compound was obtained as a white solid, yield 17%; m.p. = 78 – 79 °C. 1H -NMR (300 MHz, $CDCl_3$) δ (ppm): 2.30 – 2.56 (m, 10H, 2H CH_2CH_2 piperazine + 8H piperazine), 3.39 (q, $J = 5.7$ Hz, 2H, $NHCH_2CH_2$), 3.49 (s, 2H, Piperazine CH_2Ph), 4.45 (s, 2H, OCH_2CO), 3.77 (s, 3H, OCH_3), 6.79 – 6.90 (m, 4H aromatics), 7.10 – 7.19 (bs, 1H, NH), 7.22 – 7.35 (m, 5H aromatics). ^{13}C NMR (126 MHz, $CDCl_3$) δ (ppm): 35.50, 52.71, 53.09, 55.69, 56.08, 63.03, 68.14, 114.84, 115.60, 127.03, 128.08, 129.15, 138.04, 151.51, 154.66, 168.38. UPLC: $t_R = 5.4$ min; HRMS ($C_{22}H_{29}N_3O_3+H^+$): calculated 384.2282 found 384.2288.

N-(2-(4-Benzylpiperazin-1-yl)ethyl)-2-(4-chlorophenoxy)acetamide (**20**)

Starting from 2-(4-chlorophenoxy)acetic acid (**10a**) and 2-(4-benzyl-1-piperazine-1-yl)ethanamine (**22**), eluent: CH₂Cl₂/MeOH 95:5, then 100% EtOAc. The title compound was obtained as a white solid, yield 23%; m.p. = 87 – 88 °C. ¹H NMR (300 MHz, CDCl₃) δ (ppm): 2.36 – 2.43 (m, 10H, 2H CH₂CH₂piperazine + 8H piperazine), 3.31 (q, J = 5.3 Hz, 2H, NHCH₂CH₂), 3.42 (s, 2H, piperazineCH₂Ph), 4.40 (s, 2H, OCH₂CO), 6.75 – 6.78 (m, 2H aromatics), 7.02 (bs, 1H, NH), 7.18 – 7.23 (m, 7H aromatics). ¹³C NMR (125 MHz, CDCl₃) δ (ppm): 35.47, 52.68, 53.04, 55.93, 63.00, 67.63, 115.92, 126.99, 127.05, 128.19, 129.17, 129.66, 137.94, 155.93, 167.64. UPLC: t_R = 8.8 min; HRMS (C₂₁H₂₆ClN₃O₂+H⁺): calculated 388.1786 found 388.1788.

Biological Methods

AChE and BChE Inhibition

A previously described modified protocol of Ellman's spectrophotometric assay [62], adapted to a 96-well plate procedure, was used [63]. All reagents and enzymes were from Sigma-Aldrich, (Milan, Italy). Incubations were carried out in clear flat-bottomed, 96-well plates (Greiner Bio-One GmbH, Frickenhausen, Germany) in duplicate. For most active compounds (inhibition > 60%), IC₅₀ was determined from seven solutions (ranging from 10⁻⁵ to 10⁻¹¹ M as the final concentrations) of inhibitor and prepared by diluting a stock DMSO solution 1000 μM with the work buffer. Plate readings were made with Infinite M1000 Pro multiplate reader (Tecan, Cernusco S.N., Italy). IC₅₀ values and inhibition values were calculated with the software GraphPad Prism as the mean of three independent experiments and are expressed as mean ± SEM.

Inhibition of Aβ₄₀ Aggregation

The spectrofluorimetric assays measuring ThT fluorescence in the presence of Aβ were performed as previously described [63]. Co-incubation samples were prepared in 96-well black, non-binding

microplates (Greiner Bio-One GmbH, Frickenhausen, Germany) by diluting A β ₄₀ (EZBiolab, Carmel, IN, USA) and inhibitors to a final concentration of 30 and 100 μ M respectively in PBS (pH 7.4) containing 2% 1,1,1,3,3,3-hexafluoro-2-propanol (HFIP). After 2 h of incubation at 25 °C, 25 μ M ThT solution was added and fluorescence was determined with a multi-plate reader Infinite M1000 Pro (Tecan, Cernusco S.N., Italy). Assays were carried out in triplicate and values are reported as mean \pm SEM.

FAAH Inhibition

FAAH inhibition assays were performed in triplicate using 96-well black flat-bottom microtiter NBS plates (COSTAR flat black). In a total volume of 200 μ L, different concentrations of each potential inhibitor were preincubated in an appropriate fluorometric assay buffer (tris-HCl 125 mM, Na₂EDTA \cdot 2H₂O 1 mM, pH = 9.0) with the enzyme (FAAH Human recombinant, Cayman Chemical, Ann Arbor, MI, USA) for 10 min at room temperature, maintaining the plate in orbital shaking. The substrate (7-amino-4-methyl-2H-1-benzopyran-2-one-5Z,8Z,11Z,14Z-eicosatetraenamide, AMC-AA, 5 μ M final concentration) was then added, and the assay was incubated for 2h at 37 °C in a TECAN infinite M1000Pro plate reader (Tecan, Männedorf, Switzerland) which read the fluorescence from each well every 30s (λ_{ex} = 340 nm, λ_{em} = 450 nm), expressing FAAH activity as relative fluorescence units (RFU). Percent inhibition for each tested compound were calculated using control wells lacking the inhibitor and blank wells lacking both inhibitor and enzyme. IC₅₀ values were calculated using GraphPad Prism 5.0 (GraphPad Software, La Jolla, CA, USA) and are expressed as mean \pm SEM of at least two independent measurements performed in triplicate.

Cell Cultures.

SH-SY5Y neuroblastoma cells and human HepG2 hepatocarcinoma cells were obtained from American Type Culture Collection (ATCC®, Bethesda, MD). SH-SY5Y cells were cultured in a 1:1 mixture of MEM and Ham's F12 Medium supplemented with 10% (v/v) heat-inactivated Fetal Bovine Serum, 1% (v/v) Glutamine and 1% (v/v) Penicillin – Streptomycin. HepG2 cells were

cultured in MEM supplemented with 10% (v/v) heat-inactivated Fetal Bovine Serum, 1% (v/v) Glutamine and 1% (v/v) Penicillin – Streptomycin, 1% (v/v) NEAA. Cells were cultivated at 37 °C with 5% CO₂ at saturated humidity.

Cell Viability

Cell Viability was evaluated via MTT assay at 24 and 48 h from treatment. On day 1, 10,000-25,000 cells/well were seeded into 96-well plates in a volume of 100 µL. On day 2, the medium was replaced with one containing serial dilutions at a half-log factor of the test compounds (from 100 µM to 100 nM). Test compounds were dissolved in DMSO (1% final concentration). Control wells lacking treatment were included in the experimental design. After the established incubation time with drugs (24-48 h), MTT (0.5 mg/mL) was added to each well, and after 3–4 h incubation at 37 °C, the supernatant was removed. The formazan crystals were solubilized using 100 µl of DMSO/EtOH (1:1) and the absorbance values at 570 nm were determined on the Victor 3 microplate reader from PerkinElmer Life Sciences. IC₅₀ values were determined from dose–response curves using GraphPad PRISM (version 5.0).

Docking studies

For each of the examined compounds the relative SMILES string was converted to three-dimensional structure within Maestro software package [64]. The proper ionization was then assigned with *fixpka* complement of QUACPAC [65], and thereafter the molecular skeleton was minimized performing a 10000 steps of Steepest Descent with Open Babel [66] using the Universal Force Field. Enzyme-inhibitor complexes of AChE (chain A; pdb code 6O4W) [67], BChE (pdb code 7AZM) [68], and FAAH (pdb code 4DO3) [69] X-ray structures were selected as targets for dockings, and then prepared with the Protein Preparation Wizard interface of Maestro removing the ligand and water molecules, adding hydrogen atoms, optimizing their position, and assigning the ionization states of acid and basic residues according to PROPKA prediction at pH 7.0. Electrostatic charges for proteins atoms were loaded according to AMBER UNITED force field [70], while the

molcharge complement of QUACPAC [65] was used in order to achieve Marsili-Gasteiger charges for the inhibitors. Affinity maps for each enzyme were first calculated on a 0.375 Å spaced 85×85×85 Å³ cubic box, having the barycentre on the co-crystallized inhibitors poses, and the binding site available space was tested throughout 1000 runs of Lamarckian Genetic Algorithm (LGA) implemented in AUTODOCK 4.2.6 [71] using the GPU-OpenCL algorithm version [72]. The hydration force field parameters [73] were set in order to explicitly evaluate water molecules contribution in the binding, and the population size and the number of energy evaluation figures were set to 300 and 10000000, respectively. Filtering of the docking poses was achieved by an energy-, similarity- and population-based rule, we called **ESP**, where **E** accounts for the free energy of binding, the energy difference between the selected pose and the relative global minimum and the ligand efficacy, **S** the similarity as scored by the Tanimoto_Combo coefficient according to the shape matching algorithm ROCS [74], **P** is the cluster member population.

Complexation Studies

Materials and equipment

The aqueous copper (CuCl₂, 0.015 M) stock solution was prepared from a 1000 ppm Titrisol standard and the respective copper content was evaluated by atomic absorption. The 0.076 M HCl solution, used in pH-potentiometric and spectrophotometric titrations, was prepared from a Titrisol ampoule while the titrant (KOH 0.08 M) was from carbonate free commercial concentrate (Titrisol ampoule). The KOH solution was standardized by titration with a solution of potassium hydrogen phthalate and was discarded whenever the percentage of carbonate, determined by Gran's method [75] was greater than 1% of the total amount of base.

The ¹H NMR spectra were recorded on a Bruker AVANCE III-400 (400 MHz) NMR spectrometer, at 25 °C, and chemical shifts (δ) are reported in ppm from the DMSO peak. Mass spectra were

recorded on an LCQ FleetTM ion trap mass spectrometer equipped with an ESI ion source operated in positive and negative ion modes (Thermo Scientific).

Potentiometric studies

Copper complexation studies were performed by pH-potentiometric titration and the experimental conditions were analogous to those previously reported [76]. Titration of compound **12**, alone or in the presence of Cu²⁺, was accomplished in a 30% w/w DMSO/H₂O medium, at $T = 25.0 \pm 0.1$ °C and ionic strength (I) 0.1 M KCl, by using 0.08 M KOH as titrant. The glass and Ag/AgCl reference electrodes were previously conditioned for some days in several DMSO/H₂O mixtures of increasing DMSO % composition and the response of the glass electrode was checked by strong acid – strong base (HCl/KOH) calibrations and analysis of the respective Nernst parameters by Gran's method [75]. The ligand concentration (C_L) was 4.4×10^{-4} M, C_{Cu}/C_L ratios were 0:1, 1:1 and 1:2 and the value determined for the water ionization constant (pK_w) was 14.66. The stepwise protonation constants of the ligands, $K_i = [H_iL]/[H_{i-1}L][H]$ ($i = 1-2$), and the overall Cu²⁺-complex stability constants, $\beta_{M_mH_hL_l} = [M_mH_hL_l]/[M]^m[H]^h[L]^l$, were calculated by fitting the pH-potentiometric data with Hyperquad 2008 [51] program. The Cu²⁺ hydrolysis model was determined under the defined experimental conditions ($I = 0.1$ M KCl, 30% w/w DMSO/H₂O, $T = 25.0 \pm 0.1$ °C) and the following value of stability constant was included in the fitting of experimental data for the Cu²⁺/L system: $\log\beta_{Cu_2H_{-2}} = -9.94$. The species distribution curves were obtained with the Hyss program [51].

¹H-NMR studies

Proton NMR titrations of compound **12** (**SON38**) and the system Zn²⁺/**12** 1:1 ($C_L = 4.5$ mM) in 75% d₆-DMSO /D₂O medium were performed by using DCl or CO₂ free KOD solutions and **a**

Thermo ORION model 420 instrument fitted with a combined Mettler Toledo U402-M3-S7/200 microelectrode. The NMR titrations of **12** and Zn²⁺/**12** 1:1 system were only used to evaluate, respectively, the sequence of protonation of the ligand and to identify the metal coordination core. Therefore, no complications arise associated to the use of a medium different from that of the potentiometric studies. The microelectrode was calibrated with standard buffered aqueous solutions (pH 4 and 7) and pH* corresponds to the reading of the pH meter previously calibrated with aqueous buffers [77].

ESI-MS spectra

The pH of the Cu²⁺/**12** (**SON38**) 1:1 and 1:2 systems ($C_L = 2.6 \times 10^{-4}$ M) in 30% w/w DMSO/H₂O medium was ascertained to 5.68 and 5.73, respectively, and the respective mass spectra were obtained from a LCQ FleetTM ion trap mass spectrometer equipped with an ESI ion source operated in positive and negative ion modes (Thermo Scientific). The mass spectrometer was operated in the ESI positive/negative ion modes, with the following optimized parameters: ion spray voltage, ± 4.5 kV; capillary voltage, 16/-18 V; tube lens offset, -63/58 V, sheath gas (N₂), 80 arbitrary units; auxiliary gas, 5 arbitrary units; capillary temperature, 280 °C. Spectra typically correspond to the average of 20–35 scans and were recorded in the range between 100-1000 Da. Data acquisition and processing were performed using the Xcalibur software. The theoretical isotopic distributions were simulated by Compass Isotopic Pattern software by Bruker.

Prediction of pharmacokinetic properties

Optimized structures of the compounds were obtained in Maestro, and their pharmacokinetic properties were subsequently predicted using the software QikProp v.2.5 [78] for parameters clogP

(lipophilic character), logBB (the capacity to cross the blood-brain barrier), Caco-2 permeability (velocity of intestinal absorption), activity in the CNS, and Lipinski's rule of 5.

Acknowledgements

This work was financially supported by the University of Bari Aldo Moro and Italian Ministry of University and Research (M.U.R.). The authors from Instituto Superior Técnico / University of Lisbon received financial support from Fundação para a Ciência e Tecnologia (FCT), projects UIDB/00100/2020, UIDP/00100/2020 and LA/P/0056/2020. Acknowledgements are also due to the Portuguese NMR (IST-UL Center) and Mass Spectrometry Networks (Node IST-CTN), for providing access to their facilities, as well as to Dr Conceição Oliveira for the collaboration in the mass spectra interpretation.

Author Contributions

#L.B. and R.L. contributed equally to this work.

L.P. conceived and designed the experiments, L.B, R.L., A.C., M.C., S.O., G.V., L.G., H.B., S.C. and A.L. carried out the experimental work (R.L., S.O. and G.V. synthesis, L.B., M.C., and A.L. biological assays, A.C. and H.B. in silico studies, L.G. UPLC analyses). L.P., L.G., A.L., C.D.A., M.A.S., P.T. and F.L. provided reagents/materials/analysis tools. L.P., S.C., A.C. analyzed the data and participated in the discussion of the obtained results; L.B., R.L., M.C., S.C., A.C. and L.P. wrote the first draft of the paper. L.B., R.L., C.D.A., P.T., M.A.S., F.L. and L.P. revised the final draft of the paper. All authors have read and agreed to the published version of the manuscript. All authors have approved the final version of the manuscript.

Supplementary Materials

Overlay of the docking poses for compounds **2-4**, **12**, **13**, **18** and **20** from AChE dockings (Figure S1); Detailed view of the most populated cluster for compounds **15** and **16** posed in the BChE active site (Figure S2); ¹H-NMR and ¹³C-NMR spectra of compounds **1-20** (Figure S3); UPLC traces of sample compounds (Figure S4); Inhibition of self-mediated Aβ40 aggregation of compounds **1-20** (Table S1); Molecular descriptors used in the QSAR models (Table S2); Summary of the docking results for the AChE inhibitors (Table S3); predicted ADME properties of compounds **1-20** (Table S4).

Corresponding Authors Information

*Luca Piemontese, PhD. Dipartimento di Farmacia-Scienze del Farmaco, Università degli Studi di Bari “Aldo Moro”, Via E. Orabona 4, 70125 Bari, Italy; e-mail: luca.piemontese@uniba.it

References

- [1] 2019 Alzheimer’s disease facts and figures, *Alzheimer’s Dement.* 15 (2019) 321–387. <https://doi.org/10.1016/j.jalz.2019.01.010>.
- [2] K. Blennow, H. Zetterberg, Biomarkers for Alzheimer’s disease: current status and prospects for the future, *J. Intern. Med.* 284 (2018) 643–663. <https://doi.org/10.1111/JOIM.12816>.
- [3] Y. Zhao, B. Zhao, Oxidative stress and the pathogenesis of alzheimer’s disease, *Oxid. Med. Cell. Longev.* 2013 (2013). <https://doi.org/10.1155/2013/316523>.

- [4] R. Leuci, L. Brunetti, A. Laghezza, F. Liodice, P. Tortorella, L. Piemontese, Importance of biometals as targets in medicinal chemistry: An overview about the role of zinc (II) chelating agents, *Appl. Sci.* 10 (2020) 4118. <https://doi.org/10.3390/APP10124118>.
- [5] İ. Gulcin, S.H. Alwasel, Metal Ions, Metal Chelators and Metal Chelating Assay as Antioxidant Method, *Process.* 2022, Vol. 10, Page 132. 10 (2022) 132. <https://doi.org/10.3390/PR10010132>.
- [6] İ. Gulcin, Antioxidants and antioxidant methods: an updated overview, *Arch. Toxicol.* 94 (2020) 651–715. <https://doi.org/10.1007/S00204-020-02689-3>.
- [7] Y. Liu, M. Nguyen, A. Robert, B. Meunier, Metal Ions in Alzheimer's Disease: A Key Role or Not?, *Acc. Chem. Res.* 52 (2019) 2026–2035. <https://doi.org/10.1021/ACS.ACCOUNTS.9B00248>.
- [8] M.A. Lovell, J.D. Robertson, W.J. Teesdale, J.L. Campbell, W.R. Markesbery, Copper, iron and zinc in Alzheimer's disease senile plaques, *J. Neurol. Sci.* 158 (1998) 47–52. [https://doi.org/10.1016/S0022-510X\(98\)00092-6](https://doi.org/10.1016/S0022-510X(98)00092-6).
- [9] A.I. Bush, R.E. Tanzi, Therapeutics for Alzheimer's disease based on the metal hypothesis, *Neurotherapeutics.* 5 (2008) 421. <https://doi.org/10.1016/J.NURT.2008.05.001>.
- [10] A.R. White, K.M. Kanninen, P.J. Crouch, Editorial: Metals and neurodegeneration: restoring the balance, *Front. Aging Neurosci.* 7 (2015) 127. <https://doi.org/10.3389/FNAGI.2015.00127>.
- [11] S. Chaves, K. Várnagy, M.A. Santos, Recent Multi-target Approaches on the Development of Anti-Alzheimer's Agents Integrating Metal Chelation Activity, *Curr. Med. Chem.* 28 (2021) 7247–7277. <https://doi.org/10.2174/0929867328666210218183032>.
- [12] V. Van Der Velpen, T. Teav, H. Gallart-Ayala, F. Mehl, I. Konz, C. Clark, A. Oikonomidi, G. Peyratout, H. Henry, M. Delorenzi, J. Ivanisevic, J. Popp, Systemic and central nervous system metabolic alterations in Alzheimer's disease, *Alzheimer's Res. Ther.* 11 (2019). <https://doi.org/10.1186/s13195-019-0551-7>.

- [13] B.J. Neth, S. Craft, Insulin Resistance and Alzheimer's Disease: Bioenergetic Linkages, *Front. Aging Neurosci.* 9 (2017). <https://doi.org/10.3389/fnagi.2017.00345>.
- [14] G. Esposito, C. Scuderi, C. Savani, L. Steardo, D. De Filippis, P. Cottone, T. Iuvone, V. Cuomo, L. Steardo, Cannabidiol in vivo blunts beta-amyloid induced neuroinflammation by suppressing IL-1beta and iNOS expression, *Br. J. Pharmacol.* 151 (2007) 1272–1279. <https://doi.org/10.1038/sj.bjp.0707337>.
- [15] S.S. Duffy, J.P. Hayes, N.T. Fiore, G. Moalem-Taylor, The cannabinoid system and microglia in health and disease, *Neuropharmacology.* 190 (2021). <https://doi.org/10.1016/j.neuropharm.2021.108555>.
- [16] B.S. Basavarajappa, M. Shivakumar, V. Joshi, S. Subbanna, Endocannabinoid system in neurodegenerative disorders, *J. Neurochem.* 142 (2017) 624–648. <https://doi.org/10.1111/jnc.14098>.
- [17] A.J. Berry, O. Zubko, S.J. Reeves, R.J. Howard, Endocannabinoid system alterations in Alzheimer's disease: A systematic review of human studies, *Brain Res.* 1749 (2020). <https://doi.org/10.1016/j.brainres.2020.147135>.
- [18] G. Bedse, A. Romano, A.M. Lavecchia, T. Cassano, S. Gaetani, The role of endocannabinoid signaling in the molecular mechanisms of neurodegeneration in Alzheimer's disease, *J. Alzheimer's Dis. JAD.* 43 (2015) 1115–1136. <https://doi.org/10.3233/JAD-141635>.
- [19] J. Fernández-Ruiz, J. Romero, J.A. Ramos, Endocannabinoids and Neurodegenerative Disorders: Parkinson's Disease, Huntington's Chorea, Alzheimer's Disease, and Others, *Handb. Exp. Pharmacol.* 231 (2015) 233–259. https://doi.org/10.1007/978-3-319-20825-1_8.
- [20] S. Agarwal, A. Yadav, R.K. Chaturvedi, Peroxisome proliferator-activated receptors (PPARs) as therapeutic target in neurodegenerative disorders, *Biochem. Biophys. Res. Commun.* 483 (2017) 1166–1177. <https://doi.org/10.1016/j.bbrc.2016.08.043>.
- [21] L. Brunetti, A. Laghezza, F. Liodice, P. Tortorella, L. Piemontese, Combining fatty acid amide hydrolase (FAAH) inhibition with peroxisome proliferator-activated receptor (PPAR)

activation: A new potential multi-target therapeutic strategy for the treatment of Alzheimer's disease, *Neural Regen. Res.* 15 (2020) 67–68. <https://doi.org/10.4103/1673-5374.264458>.

- [22] L. Piemontese, An innovative approach for the treatment of Alzheimer's disease: The role of peroxisome proliferator-activated receptors and their ligands in development of alternative therapeutic interventions, *Neural Regen. Res.* 14 (2019) 43–45. <https://doi.org/10.4103/1673-5374.241043>.
- [23] R. Leuci, L. Brunetti, A. Laghezza, L. Piemontese, A. Carrieri, L. Pisani, P. Tortorella, M. Catto, F. Liodice, A New Series of Aryloxyacetic Acids Endowed with Multi-Target Activity towards Peroxisome Proliferator-Activated Receptors (PPARs), Fatty Acid Amide Hydrolase (FAAH), and Acetylcholinesterase (AChE), *Mol.* 2022, Vol. 27, Page 958. 27 (2022) 958. <https://doi.org/10.3390/MOLECULES27030958>.
- [24] L. Cristino, T. Bisogno, V. Di Marzo, Cannabinoids and the expanded endocannabinoid system in neurological disorders, *Nat. Rev. Neurol.* 16 (2020) 9–29. <https://doi.org/10.1038/s41582-019-0284-z>.
- [25] S. Jain, A. Bisht, K. Verma, S. Negi, S. Paliwal, S. Sharma, The role of fatty acid amide hydrolase enzyme inhibitors in Alzheimer's disease, *Cell Biochem. Funct.* (2021). <https://doi.org/10.1002/cbf.3680>.
- [26] V. Chiurchiù, L. Scipioni, B. Arosio, D. Mari, S. Oddi, M. Maccarrone, Anti-inflammatory effects of fatty acid amide hydrolase inhibition in monocytes/macrophages from Alzheimer's disease patients, *Biomolecules.* 11 (2021). <https://doi.org/10.3390/biom11040502>.
- [27] H. Göcer, A. Akincioğlu, S. Göksu, I. Gülçin, C.T. Supuran, Carbonic anhydrase and acetylcholinesterase inhibitory effects of carbamates and sulfamoylcarbamates, *J. Enzyme Inhib. Med. Chem.* 30 (2015) 316–320. <https://doi.org/10.3109/14756366.2014.928704>.
- [28] A. Akincioğlu, H. Akincioğlu, I. Gülçin, S. Durdagi, C.T. Supuran, S. Göksu, Discovery of potent carbonic anhydrase and acetylcholine esterase inhibitors: novel sulfamoylcarbamates and sulfamides derived from acetophenones, *Bioorg. Med. Chem.* 23 (2015) 3592–3602.

<https://doi.org/10.1016/J.BMC.2015.04.019>.

- [29] F. Mangialasche, A. Solomon, B. Winblad, P. Mecocci, M. Kivipelto, Alzheimer's disease: clinical trials and drug development, *Lancet Neurol.* 9 (2010) 702–716. [https://doi.org/10.1016/S1474-4422\(10\)70119-8](https://doi.org/10.1016/S1474-4422(10)70119-8).
- [30] M.J. Oset-Gasque, J. Marco-Contelles, Alzheimer's Disease, the “one-Molecule, One-Target” Paradigm, and the Multitarget Directed Ligand Approach, *ACS Chem. Neurosci.* 9 (2018) 401–403. <https://doi.org/10.1021/acschemneuro.8b00069>.
- [31] M. Rosini, E. Simoni, R. Caporaso, A. Minarini, Multitarget strategies in Alzheimer's disease: Benefits and challenges on the road to therapeutics, *Future Med. Chem.* 8 (2016) 697–711. <https://doi.org/10.4155/fmc-2016-0003>.
- [32] E. Zanforlin, G. Zagotto, G. Ribaldo, An Overview of New Possible Treatments of Alzheimer's Disease, Based on Natural Products and Semi-Synthetic Compounds, *Curr. Med. Chem.* 24 (2017). <https://doi.org/10.2174/0929867324666170712161829>.
- [33] V. Poliseno, S. Chaves, L. Brunetti, F. Liodice, A. Carrieri, A. Laghezza, P. Tortorella, J.D. Magalhães, S.M. Cardoso, M.A. Santos, L. Piemontese, Derivatives of tenuazonic acid as potential new multi-target anti-alzheimer's disease agents, *Biomolecules.* 11 (2021) 1–23. <https://doi.org/10.3390/biom11010111>.
- [34] M.F. Maleki, H. Nadri, M. Kianfar, N. Edraki, F. Eisvand, R. Ghodsi, S.A. Mohajeri, F. Hadizadeh, Design and synthesis of new carbamates as inhibitors for fatty acid amide hydrolase and cholinesterases: Molecular dynamic, in vitro and in vivo studies, *Bioorg. Chem.* 109 (2021) 104684. <https://doi.org/10.1016/j.bioorg.2021.104684>.
- [35] S. Montanari, M. Allarà, L. Scalvini, M. Kostrzewa, F. Belluti, S. Gobbi, M. Naldi, S. Rivara, M. Bartolini, A. Ligresti, A. Bisi, A. Rampa, New Coumarin derivatives as cholinergic and cannabinoid system modulators, *Molecules.* 26 (2021) 3254. <https://doi.org/10.3390/molecules26113254>.
- [36] L. Brunetti, A. Carrieri, L. Piemontese, P. Tortorella, F. Liodice, A. Laghezza, Beyond the

- canonical endocannabinoid system. A screening of ppar ligands as FAAH inhibitors, *Int. J. Mol. Sci.* 21 (2020) 1–20. <https://doi.org/10.3390/ijms21197026>.
- [37] S. Chaves, S. Resta, F. Rinaldo, M. Costa, R. Josselin, K. Gwizdala, L. Piemontese, V. Capriati, A.R. Pereira-Santos, S.M. Cardoso, M.A. Santos, Design, synthesis, and in vitro evaluation of hydroxybenzimidazole-donepezil analogues as multitarget-directed ligands for the treatment of Alzheimer's disease, *Molecules*. 25 (2020). <https://doi.org/10.3390/molecules25040985>.
- [38] L. Piemontese, D. Tomás, A. Hiremathad, V. Capriati, E. Candeias, S.M. Cardoso, S. Chaves, M.A. Santos, Donepezil structure-based hybrids as potential multifunctional anti-Alzheimer's drug candidates, *J. Enzyme Inhib. Med. Chem.* 33 (2018) 1212–1224. <https://doi.org/10.1080/14756366.2018.1491564>.
- [39] F. Queda, S. Calò, K. Gwizdala, J.D. Magalhães, S.M. Cardoso, S. Chaves, L. Piemontese, M.A. Santos, Novel Donepezil–Arylsulfonamide Hybrids as Multitarget-Directed Ligands for Potential Treatment of Alzheimer's Disease, *Mol.* 2021, Vol. 26, Page 1658. 26 (2021) 1658. <https://doi.org/10.3390/MOLECULES26061658>.
- [40] A. Hiremathad, L. Piemontese, Heterocyclic compounds as key structures for the interaction with old and new targets in Alzheimer's disease therapy, *Neural Regen. Res.* 12 (2017) 1256–1261. <https://doi.org/10.4103/1673-5374.213541>.
- [41] L. Piemontese, R. Sergio, F. Rinaldo, L. Brunetti, F.M. Perna, M. Amélia Santos, V. Capriati, Deep Eutectic Solvents as Effective Reaction Media for the Synthesis of 2-Hydroxyphenylbenzimidazole-based Scaffolds en Route to Donepezil-Like Compounds, *Molecules*. 25 (2020). <https://doi.org/10.3390/molecules25030574>.
- [42] L. Porcelli, F. Gilardi, A. Laghezza, L. Piemontese, N. Mitro, A. Azzariti, F. Altieri, L. Cervoni, G. Fracchiolla, M. Giudici, U. Guerrini, A. Lavecchia, R. Montanari, C. Di Giovanni, A. Paradiso, G. Pochetti, G.M. Simone, P. Tortorella, M. Crestani, F. Liodice, Synthesis, characterization and biological evaluation of ureidofibrate-like derivatives

- endowed with peroxisome proliferator-activated receptor activity, *J. Med. Chem.* 55 (2012) 37–54. <https://doi.org/10.1021/jm201306q>.
- [43] L. Piemontese, G. Vitucci, M. Catto, A. Laghezza, F.M. Perna, M. Rullo, F. Loiodice, V. Capriati, M. Solfrizzo, Natural scaffolds with multi-target activity for the potential treatment of Alzheimer's disease, *Molecules*. 23 (2018). <https://doi.org/10.3390/molecules23092182>.
- [44] G. Fancellu, K. Chand, D. Tomás, E. Orlandini, L. Piemontese, D.F. Silva, S.M. Cardoso, S. Chaves, M.A. Santos, Novel tacrine–benzofuran hybrids as potential multi-target drug candidates for the treatment of Alzheimer's Disease, *J. Enzyme Inhib. Med. Chem.* 35 (2020) 211–226. <https://doi.org/10.1080/14756366.2019.1689237>.
- [45] M.A. Silva, A.S. Kiametis, W. Treptow, Donepezil Inhibits Acetylcholinesterase via Multiple Binding Modes at Room Temperature, *J. Chem. Inf. Model.* 60 (2020) 3463–3471. <https://doi.org/10.1021/acs.jcim.9b01073>.
- [46] D.K. Giang, B.F. Cravatt, Molecular characterization of human and mouse fatty acid amide hydrolases, *Proc. Natl. Acad. Sci. U. S. A.* 94 (1997) 2238–2242. <https://doi.org/10.1073/PNAS.94.6.2238>.
- [47] M.K. McKinney, B.E. Cravatt, Structure and function of fatty acid amide hydrolase, *Annu. Rev. Biochem.* 74 (2005) 411–432. <https://doi.org/10.1146/ANNUREV.BIOCHEM.74.082803.133450>.
- [48] M. Mileni, D.S. Johnson, Z. Wang, D.S. Everdeen, M. Liimatta, B. Pabst, K. Bhattacharya, R.A. Nugent, S. Kamtekar, B.F. Cravatt, K. Ahn, R.C. Stevens, Structure-guided inhibitor design for human FAAH by interspecies active site conversion, *Proc. Natl. Acad. Sci. U. S. A.* 105 (2008) 12820–12824. <https://doi.org/10.1073/PNAS.0806121105>.
- [49] A. Daina, V. Zoete, A BOILED-Egg To Predict Gastrointestinal Absorption and Brain Penetration of Small Molecules, *ChemMedChem.* 11 (2016) 1117–1121. <https://doi.org/10.1002/CMDC.201600182>.
- [50] H. Pajouhesh, G.R. Lenz, Medicinal chemical properties of successful central nervous system

drugs, *NeuroRx*. 2 (2005) 541–553. <https://doi.org/10.1602/NEURORX.2.4.541>.

- [51] P. Gans, A. Sabatini, A. Vacca, Investigation of equilibria in solution. Determination of equilibrium constants with the HYPERQUAD suite of programs, *Talanta*. 43 (1996) 1739–1753. [https://doi.org/10.1016/0039-9140\(96\)01958-3](https://doi.org/10.1016/0039-9140(96)01958-3).
- [52] H.M. Irving, M.G. Miles, L.D. Pettit, A study of some problems in determining the stoichiometric proton dissociation constants of complexes by potentiometric titrations using a glass electrode, *Anal. Chim. Acta*. 38 (1967) 475–488. [https://doi.org/10.1016/S0003-2670\(01\)80616-4](https://doi.org/10.1016/S0003-2670(01)80616-4).
- [53] M.A. Santos, M.A. Esteves, M.C.T. Vaz, M.L.S.S. Gonçalves, A new iron(III) ion sequestering ligand: synthesis, solution chemistry and electrochemistry, *J. Chem. Soc. Dalton Trans.* (1993) 927–932. <https://doi.org/10.1039/DT9930000927>.
- [54] M.A. Santos, M.A. Esteves, M.C.T. Vaz, M.L.S. Simões Gonçalves, Siderophore analogues. Chelating properties of a new cyclic diazadihydroxamic acid, *Inorganica Chim. Acta*. 214 (1993) 47–55. [https://doi.org/10.1016/S0020-1693\(00\)87525-8](https://doi.org/10.1016/S0020-1693(00)87525-8).
- [55] F.G. Mann, H.R. Watson, 565. The constitution of complex metallic salts. Part XVIII. The chelated metallic derivatives of NNN'N'-tetramethylethylene-diamine and of 1:4-dimethylpiperazine, *J. Chem. Soc.* (1958) 2772–2780. <https://doi.org/10.1039/JR9580002772>.
- [56] A. Marzotto, D.A. Clemente, F. Benetollo, G. Valle, Piperazine (and derivatives) copper(II) compounds: 1,4-dimethylpiperazin-1,4-ium tetrachlorocuprate(II) and Cu-N bond formation in trichloro(1-methylpiperazin-1-ium-N4)copper(II) and trichloro(1,4-dimethylpiperazin-1-ium-N4)copper(II), *Polyhedron*. 20 (2001) 171–177. [https://doi.org/10.1016/S0277-5387\(00\)00604-5](https://doi.org/10.1016/S0277-5387(00)00604-5).
- [57] K. Bertocello, G.D. Fallon, K.S. Murray, J.H. Hodgkin, Exogenous Bridging and Nonbridging in Copper(II) Complexes of a Binucleating 2,6-Bis((N-methylpiperazino)methyl)-4-chlorophenolate Ligand. Crystal Structures and Magnetic

Properties of Bis(μ -acetato), Dinitrito, and Bis(azido) Complexes. Possible Relevanc, *Inorg. Chem.* 27 (1988) 4750–4758. <https://doi.org/10.1021/ic00299a014>.

- [58] W.G. Haanstra, W.L. Driessen, R.A.G. de Graaff, G.C. Sebregts, J. Suriano, J. Reedijk, U. Turpeinen, R. Hämäläinen, J.S. Wood, Transition metal complexes of two related pyrazole containing ligands: 3,6-dimethyl-1,8-(3,5-dimethyl-1-pyrazolyl)-3,6-diazaoctane (ddad) and 1,4-bis(2-ethyl-(3,5-dimethyl-1-pyrazolyl))-piperazine (bedp). Synthesis, spectroscopy and X-ray structures, *Inorganica Chim. Acta.* 189 (1991) 243–251. [https://doi.org/10.1016/S0020-1693\(00\)80196-6](https://doi.org/10.1016/S0020-1693(00)80196-6).
- [59] S. Chaves, A. Hiremathad, D. Tomás, R.S. Keri, L. Piemontese, M. Amélia Santos, Exploring the chelating capacity of 2-hydroxyphenyl-benzimidazole based hybrids with multi-target ability as anti-Alzheimer's agents, *New J. Chem.* 42 (2018) 16503–16515. <https://doi.org/10.1039/c8nj00117k>.
- [60] M. Costa, R. Josselin, D.F. Silva, S.M. Cardoso, N. V. May, S. Chaves, M.A. Santos, Donepezil-based hybrids as multifunctional anti-Alzheimer's disease chelating agents: Effect of positional isomerization, *J. Inorg. Biochem.* 206 (2020). <https://doi.org/10.1016/j.jinorgbio.2020.111039>.
- [61] O. Benek, J. Korabecny, O. Soukup, A Perspective on Multi-target Drugs for Alzheimer's Disease, *Trends Pharmacol. Sci.* 41 (2020) 434–445. <https://doi.org/10.1016/J.TIPS.2020.04.008>.
- [62] G.L. Ellman, K.D. Courtney, V. Andres, R.M. Featherstone, A new and rapid colorimetric determination of acetylcholinesterase activity, *Biochem. Pharmacol.* 7 (1961) 88–95. [https://doi.org/10.1016/0006-2952\(61\)90145-9](https://doi.org/10.1016/0006-2952(61)90145-9).
- [63] L. Pisani, A. De Palma, N. Giangregorio, D. V. Miniero, P. Pesce, O. Nicolotti, F. Campagna, C.D. Altomare, M. Catto, Mannich base approach to 5-methoxyisatin 3-(4-isopropylphenyl)hydrazone: A water-soluble prodrug for a multitarget inhibition of cholinesterases, beta-amyloid fibrillization and oligomer-induced cytotoxicity, *Eur. J. Pharm.*

Sci. 109 (2017) 381–388. <https://doi.org/10.1016/j.ejps.2017.08.004>.

- [64] Schrödinger LLC, Schrödinger Release 2021-1, Maestro, (2021).
- [65] QUACPAC 2.1.0.4, OpenEye Scientific Software, Santa Fe, NM, <http://www.eyesopen.com>, (n.d.). www.eyesopen.com.
- [66] N.M. O’Boyle, M. Banck, C.A. James, C. Morley, T. Vandermeersch, G.R. Hutchison, Open Babel: An Open chemical toolbox, *J. Cheminform.* 3 (2011) 33. <https://doi.org/10.1186/1758-2946-3-33>.
- [67] O. Gerlits, K.Y. Ho, X. Cheng, D. Blumenthal, P. Taylor, A. Kovalevsky, Z. Radić, A new crystal form of human acetylcholinesterase for exploratory room-temperature crystallography studies, *Chem. Biol. Interact.* 309 (2019) 108698. <https://doi.org/10.1016/J.CBI.2019.06.011>.
- [68] A. Pasieka, D. Panek, J. Jończyk, J. Godyń, N. Szałaj, G. Latacz, J. Tabor, E. Mezeiova, F. Chantegreil, J. Dias, D. Knez, J. Lu, R. Pi, J. Korabecny, X. Brazzolotto, S. Gobec, G. Höfner, K. Wanner, A. Więckowska, B. Malawska, Discovery of multifunctional anti-Alzheimer’s agents with a unique mechanism of action including inhibition of the enzyme butyrylcholinesterase and γ -aminobutyric acid transporters, *Eur. J. Med. Chem.* 218 (2021) 113397. <https://doi.org/10.1016/j.ejmech.2021.113397>.
- [69] L. Bertolacci, E. Romeo, M. Veronesi, P. Magotti, C. Albani, M. Dionisi, C. Lambruschini, R. Scarpelli, A. Cavalli, M. De Vivo, D. Piomelli, G. Garau, A binding site for nonsteroidal anti-inflammatory drugs in fatty acid amide hydrolase, *J. Am. Chem. Soc.* 135 (2013) 22–25. <https://doi.org/10.1021/ja308733u>.
- [70] C.I. Bayly, K.M. Merz, D.M. Ferguson, W.D. Cornell, T. Fox, J.W. Caldwell, P.A. Kollman, P. Cieplak, I.R. Gould, D.C. Spellmeyer, A Second Generation Force Field for the Simulation of Proteins, Nucleic Acids, and Organic Molecules, *J. Am. Chem. Soc.* 117 (1995) 5179–5197. <https://doi.org/10.1021/ja00124a002>.
- [71] G.M. Morris, D.S. Goodsell, R.S. Halliday, R. Huey, W.E. Hart, R.K. Belew, A.J. Olson, Automated docking using a Lamarckian genetic algorithm and an empirical binding free

- energy function, *J. Comput. Chem.* 19 (1998) 1639–1662.
[https://doi.org/10.1002/\(SICI\)1096-987X\(19981115\)19:14<1639::AID-JCC10>3.0.CO;2-B](https://doi.org/10.1002/(SICI)1096-987X(19981115)19:14<1639::AID-JCC10>3.0.CO;2-B).
- [72] L. El Khoury, D. Santos-Martins, S. Sasmal, J. Eberhardt, G. Bianco, F.A. Ambrosio, L. Solis-Vasquez, A. Koch, S. Forli, D.L. Mobley, Comparison of affinity ranking using AutoDock-GPU and MM-GBSA scores for BACE-1 inhibitors in the D3R Grand Challenge 4, *J. Comput. Aided. Mol. Des.* 33 (2019) 1011–1020. <https://doi.org/10.1007/s10822-019-00240-w>.
- [73] S. Forli, A.J. Olson, A force field with discrete displaceable waters and desolvation entropy for hydrated ligand docking, *J. Med. Chem.* 55 (2012) 623–638. <https://doi.org/10.1021/jm2005145>.
- [74] OpenEye Scientific Software, ROCS, 3.4.0.4, OpenEye Scientific Software, Santa Fe, NM, <http://www.eyesopen.com>, (n.d.). <http://www.eyesopen.com>.
- [75] F.J.C. Rossotti, H. Rossotti, Potentiometric titrations using gran plots: A textbook omission, *J. Chem. Educ.* 42 (1965) 375–378. <https://doi.org/10.1021/ed042p375>.
- [76] S. Chaves, A. Capelo, L. Areias, S.M. Marques, L. Gano, M.A. Esteves, M.A. Santos, A novel tripodal tris-hydroxypyrimidinone sequestering agent for trivalent hard metal ions: synthesis, complexation and in vivo studies, *Dalt. Trans.* 42 (2013) 6033–6045. <https://doi.org/10.1039/C2DT32361C>.
- [77] A. Krężel, W. Bal, A formula for correlating pKa values determined in D2O and H2O, *J. Inorg. Biochem.* 98 (2004) 161–166. <https://doi.org/10.1016/J.JINORGBIO.2003.10.001>.
- [78] QikProp 2.5, Schrödinger, New York, NY, (2005).